ICMES IN THE INNER HELIOSPHERE: ORIGIN, EVOLUTION AND PROPAGATION EFFECTS

Report of Working Group G

R. J. FORSYTH[1,*], V. BOTHMER[2], C. CID[3], N. U. CROOKER[4], T. S. HORBURY[1], K. KECSKEMETY[5], B. KLECKER[6], J. A. LINKER[7], D. ODSTRCIL[8], M. J. REINER[9], I. G. RICHARDSON[10], J. RODRIGUEZ-PACHECO[3], J. M. SCHMIDT[11] and R. F. WIMMER-SCHWEINGRUBER[12]

[1]*The Blackett Laboratory, Imperial College London, London, UK*
[2]*Institute for Astrophysics, University of Göttingen, Göttingen, Germany*
[3]*Alcalá Space Research Group, Dpto. Física, Univ. de Alcalá, Madrid, Spain*
[4]*Center for Space Physics, Boston University, Boston, Massachusetts, USA*
[5]*KFKI Research Institute for Particle and Nuclear Physics, Budapest, Hungary*
[6]*MPI für Extraterrestrische Physik, Garching, Germany*
[7]*SAIC, San Diego, CA, USA*
[8]*NOAA Space Environment Center, Boulder, CO, USA*
[9]*The Catholic University of America and NASA/GSFC, Greenbelt, MD, USA*
[10]*NASA Goddard Space Flight Center, Greenbelt, MD, USA*
[11]*International University Bremen, Bremen, Germany*
[12]*Institut für Experimentelle und Angewandte Physik, Extraterrestrische Physik, Christian-Albrechts-Universität zu Kiel, Kiel, Germany*
*(*Author for correspondence: E-mail: r.forsyth@imperial.ac.uk)*

(Received 7 February 2006; Accepted in final form 24 May 2006)

Abstract. This report assesses the current status of research relating the origin at the Sun, the evolution through the inner heliosphere and the effects on the inner heliosphere of the interplanetary counterparts of coronal mass ejections (ICMEs). The signatures of ICMEs measured by *in-situ* spacecraft are determined both by the physical processes associated with their origin in the low corona, as observed by space-borne coronagraphs, and by the physical processes occurring as the ICMEs propagate out through the inner heliosphere, interacting with the ambient solar wind. The solar and *in-situ* observations are discussed as are efforts to model the evolution of ICMEs from the Sun out to 1 AU.

Keywords: coronal mass ejections, magnetic clouds, solar wind, interplanetary shocks

1. Introduction

A fundamental problem in understanding the physics of CMEs is our limited knowledge of their physical properties. Remote sensing observations, such as those from coronagraphs, do not provide quantitative values of coronal plasma and magnetic field parameters of CMEs, while by the time that *in-situ* observations are made out in the heliosphere, ICMEs have already experienced substantial evolution and interaction with the ambient solar wind (e.g., Klein and Burlaga, 1982; Bothmer and Schwenn, 1994, 1998; Crooker and Horbury, 2006, this volume). Furthermore,

Space Science Reviews (2006) 123: 383–416
DOI: 10.1007/s11214-006-9022-0

attempts to make direct associations between *in-situ* parameters and coronagraph images suffer from the fact that those ICMEs that are intercepted by near-Earth spacecraft usually originate as Earth-directed front-side halos for which the CME structure and speed of propagation are most difficult to determine with current coronagraphs located near Earth. Another complication is that a spacecraft takes measurements along a trajectory through the ICME. In simple cases, such as a magnetic cloud, the large-scale ICME structure can be inferred from the observations assuming a suitable model, although it has to be borne in mind that such observations characterise only the middle segment near the apex of the much larger flux ropes (e.g., Figure 2 of Zurbuchen and Richardson, 2006, this volume). In other cases, in particular where the spacecraft only skims the ICME, it may be unclear how to interpret the observations in terms of ICME structure.

In this chapter, we focus on relating ICMEs to their CME origins, in particular, those origins that are assumed to involve flux rope formation (e.g., Mikic and Lee, 2006, this volume), and discuss ICME evolution with heliocentric distance, including the effects on the ambient solar wind. Important questions addressed include:

– How do the features of ICMEs observed *in-situ* reflect their solar origins?
– How does the structure of ICMEs change as they propagate through the inner heliosphere?
– How are ICMEs decelerated and/or accelerated on their journey out to 1AU?
– How do ICME shocks form and evolve?
– How do ICMEs interact with other solar wind streams, either high speed flows from coronal holes or other ICMEs, and how do compound streams form?
– What are the solar cycle variations of the above phenomena?
– Can we model ICME evolution in the inner heliosphere?

The data available for addressing these questions consists of solar observations, primarily from space-borne coronagraphs, and of *in-situ* data from various spacecraft. Sections 2 and 3 discuss ICME parameters that reflect their solar origins and how ICME parameters evolve with distance from the Sun. Section 4 addresses ICME interactions with the structured solar wind, and Section 5 describes some solar cycle variations. Section 6 discusses attempts to model CME and ICME evolution through the inner heliosphere, presenting a number of case studies. Finally, Section 7 addresses Type II radio emissions and the interplanetary scintillation technique, which provide information that bridges the gap between solar and *in-situ* observations.

2. Relating ICMEs to CMEs

V. BOTHMER, N. U. CROOKER, AND J. RODRIGUEZ-PACHECO

Research that attempts to relate features in ICMEs to features in CMEs focuses on the simplest forms of each, the ICME with flux-rope structure (e.g., Zurbuchen and

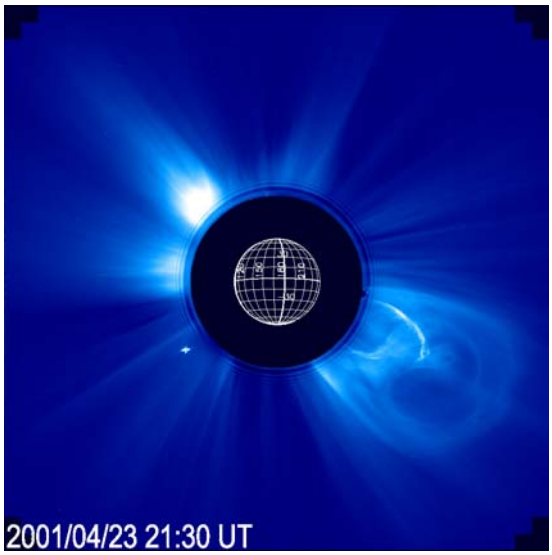

Figure 1. CME with flux-rope structure (Cremades and Bothmer, 2004).

Richardson, 2006, this volume) and the three-part CME (e.g., Hudson *et al*., 2006, this volume). This section discusses how certain aspects of these forms appear to survive the kinematic and dynamic distortions that CMEs undergo as they expand out into the spherical geometry of the heliosphere and become ICMEs.

CMEs with the typical three-part structure are made up of a leading outward moving bright front followed by a dark cavity and finally a bright core of filament plasma at its trailing edge (Hundhausen, 1988). Figure 1 from Cremades and Bothmer (2004) shows an example. While to date it is not clear how the different CME parts evolve in the heliosphere and what signatures they give in the *in-situ* data, it is generally assumed that the bright front corresponds to the sheath of compressed solar wind while the dark cavity comprises the flux rope structure observed in magnetic clouds and reflects their low gas pressure balanced by high magnetic pressure. The dark cavity in Figure 1 is a particularly good example of this expectation since its circular shape resembles the cross-section of a cylindrical flux rope. What becomes of the cool, dense filament plasma, which can cover large areas in coronagraph images, is an open question, since evidence (such as exceptionally low ion charge states) appears extremely rarely in in situ data (see Wimmer-Schweingruber *et al*., 2006, this volume, Zurbuchen and Richardson, 2006, this volume, and Crooker and Horbury, 2006, this volume).

The flux rope structure of magnetic clouds also shows what is probably the clearest imprint of the solar origin of ICMEs (see, also, Crooker and Horbury, 2006, this volume and Wimmer-Schweingruber *et al*. (this volume, cf. their Figure 6)). Figure 2 reviews how the magnetic field structure at the sites of solar prominences

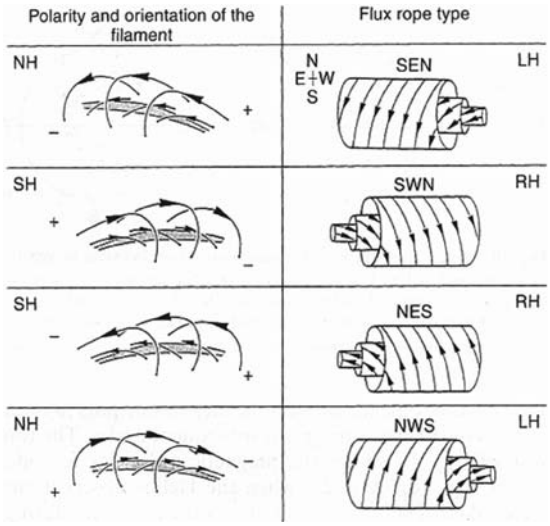

Figure 2. Magnetic field structure of solar prominences and magnetic clouds (Bothmer and Schwenn, 1994).

relates to the structure of the associated clouds according to Bothmer and Schwenn (1994). For prominences in the southern solar hemisphere, the axial field should be right-handed, independent of the solar cycle, whereas the direction of the arcade of loops overlying the prominence that later may be identified as the (I)CME's circular field lines reflects the dipolar component of the solar field, which reverses during the solar cycle. Bothmer and Schwenn (1994, 1998) and Bothmer and Rust (1997) found a good correlation between the magnetic structure at the site of disappearing filaments and the subsequent magnetic clouds (ICMEs) observed by the Helios spacecraft.

To give an example of how the pattern in Figure 2 can be tested against data, we use the well-studied event of January 1997. Figure 3 shows the *in-situ* cloud data. The rotation of the magnetic field vector varies from south to west to north. Based on this right-handed signature, one would expect the cloud to originate from the southern hemisphere. Figure 4, adapted from Bothmer (2003), shows the source region of the (I)CME. It indeed lies in the southern hemisphere, and the field polarity pattern shown in the magnetogram is consistent with a right-handed structure and a southward leading field. The cloud configuration thus agrees with the scenario proposed in Figure 2, and the source region of the CME is consistent with the results of Dere *et al*. (1999) and Cremades and Bothmer (2004), who have shown that CMEs arise from bipolar regions, either active or decaying ones, or from parts of it.

Less clear is the degree to which the tilt of the cloud axis reflects the orientation of the configuration at the source. The Yohkoh soft X-ray image on the right of Figure 4 shows hot coronal loops in the source region with enhanced magnetic flux, which are generally interpreted as evidence of reconnection in the wake of a CME, although in

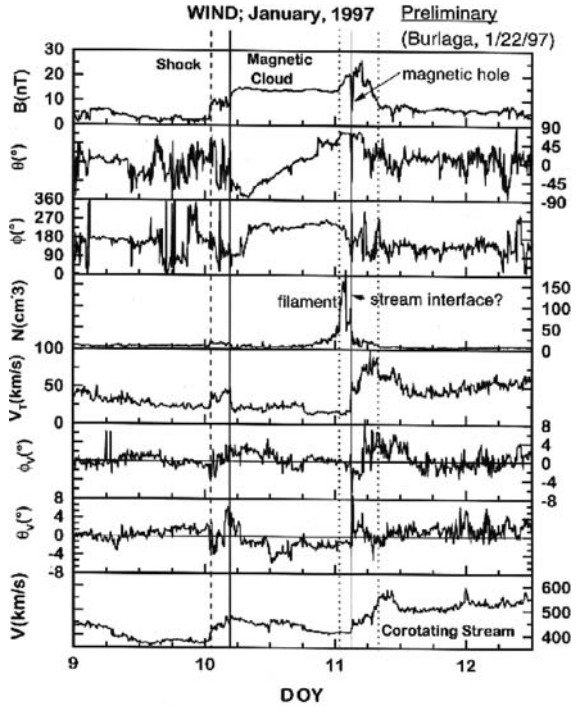

Figure 3. The magnetic cloud (ICME) in January 1997 (adapted from Burlaga *et al*., 1998).

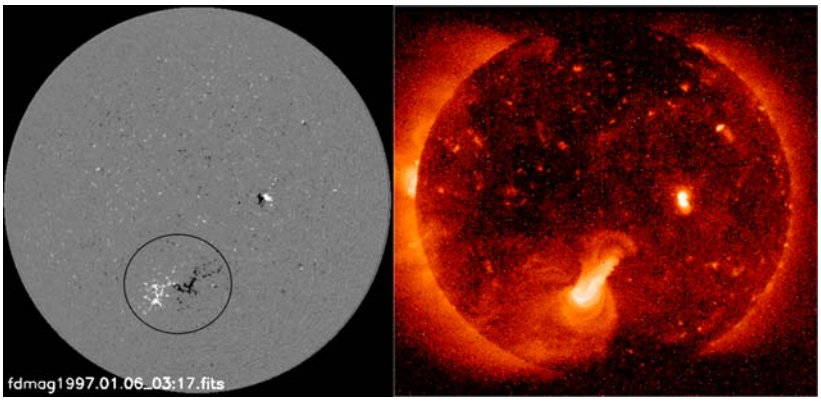

Figure 4. SOHO/MDI magnetogram (left) and Yohkoh soft X-ray images (right) showing the source region (circle) of the January 6, 1997 CME. White colors in the magnetogram indicate positive magnetic polarity (field lines pointing away from the sun).

this case the intensity of the signature was marginal (Webb *et al*., 1998). The arcade of loops arches over the neutral line between the positive and negative polarity regions in the magnetogram, and this structure presumably aligns with the flux rope that becomes the magnetic cloud. It appears to be highly inclined with respect

to the ecliptic plane, but Zhao and Hoeksema (1997) found an inclination of only 27° for the portion of the neutral line from which the associated filament erupted. From their statistically-derived relationship based upon 14 published values of filament and associated cloud-axis inclinations, they predicted a 20° cloud-axis tilt for the January 1997 event. This tilt is slightly higher than the flux-rope model results of Burlaga *et al*. (1998) and Bothmer (2003), whose values range from 3° to 15°, depending on the selected boundaries. The agreement is thus reasonably good, although cases with poor agreement have also been found (Webb *et al*., 2000). The 14 cases used by Zhao and Hoeksema (1997) yield a relatively high correlation coefficient of 0.76.

The flattening of cloud-axis tilts compared to filament tilts apparent both in the January 1997 case and in the formulation of Zhao and Hoeksema (1997) may be the result of a global deflection of CMEs toward the heliomagnetic equator by the fast solar wind emanating from coronal holes. Clear evidence for such a systematic deflection has been reported by Cremades and Bothmer (2004). At the time of the January 1997 event, polar coronal holes were present, and the CME was interacting with a fast solar wind stream. It thus created a shock wave which had not existed at the time of its lift-off (as inferred from flaring and radio wave signatures) (Burlaga *et al*., 1998). This interaction may naturally explain the flattening of the axis as observed in the heliosphere.

As reviewed by Crooker and Horbury (2006, this volume), magnetic clouds reportedly carry not only the imprint of filament axes at low solar altitudes but the imprint of the coronal streamer belt at high altitudes, as well. This tendency most likely reflects the influence of the dipolar component of the solar magnetic field, at least during the quieter phases of the solar cycle. The dipolar component dominates the helmet arcade constituting the streamer belt and is also apparent in the smaller arcades overlying the filaments, illustrated in Figure 2. During solar maximum, however, the influence of the dipolar component is apparent only far from the Sun, where the heliospheric current sheet (HCS) marking the heliomagnetic equator remains coherent on the global scale and turns over as the solar field reverses its polarity. Because of its weakness near the Sun, the overturning streamer belt may have no control over cloud axis orientation at solar maximum. Some control might be deduced from the predominance of high cloud-axis inclinations at and beyond solar maximum reported by Mulligan *et al*. (1998), following Zhao and Hoeksema (1996). On the other hand, no such predominance was found in a more recent study by Huttunen *et al*. (2005), in which high cloud-axis inclinations appear to be distributed with roughly equal probability throughout the solar cycle. The reason for these conflicting results may be due to CMEs with origins outside the helmet streamer belt, in closed-field regions surrounded by open regions of the same polarity, a configuration more common during solar maximum (Zhao and Webb, 2003; Liu and Hayashi, 2006).

Figure 5 from Rodriguez-Pacheco *et al*. (2005) supports the view that the streamer belt has little influence over magnetic cloud axes at solar maximum. On a

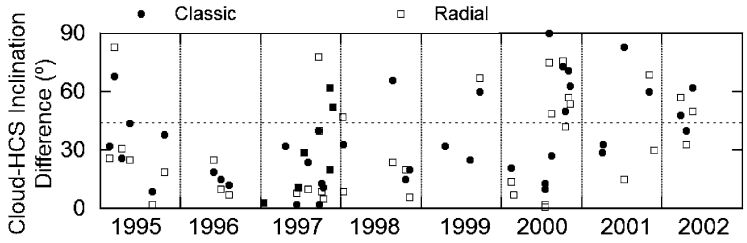

Figure 5. Differences between inclinations of magnetic cloud axes and the HCS predicted for the time of cloud encounter from classic and radial source surface maps from the Wilcox Observatory (Rodriguez-Pacheco *et al*., 2005).

case-by-case basis during the rise in activity from solar minimum (late 1996) to maximum (late 2000), Figure 5 shows that the difference between the cloud-axis inclination calculated from a force-free cylindrical flux rope model by R. P. Lepping (`http://lepmfi.gsfc.nasa.gov/mfi/mag_cloud_pub1p.html`) and the inclination of the HCS predicted from the corresponding source surface map (both classic and radial) increases substantially. The predicted HCS inclinations rise, as expected, but the cloud axis inclinations show little solar cycle variation, being predominantly low throughout the period. Although the lack of clouds with higher axis inclinations at solar maximum probably reflects a selection bias, and an unbiased data set might well show the tendency for higher elevations found by Mulligan *et al*. (1998) and Huttunen *et al*. (2005), these results clearly demonstrate that the streamer belt orientation does not govern axis inclinations of many clouds at solar maximum, consistent with the weak influence of the dipole component of the solar magnetic field at that time.

In a related effort, Blanco *et al*. (2003) reported the results of a preliminary comparison between cloud axis orientations and *in-situ*, rather than predicted, HCS orientations. They found that only about half of their 17 cases had elevation angle differences of less than 45 °, consistent with only weak streamer belt control of magnetic cloud axis orientation.

3. Evolution of ICME Parameters

I. G. RICHARDSON, C. CID, N. U. CROOKER, T. S. HORBURY, B. KLECKER, J. RODRIGUEZ-PACHECO AND R. F. WIMMER-SCHWEINGRUBER

3.1. AVERAGE PROPERTIES OF ICMES

The most comprehensive observations of ICMEs in the inner heliosphere currently available are those made by the Helios 1 and 2 spacecraft at 0.3 – 1 AU. Bothmer and Schwenn (1998) examined 46 Helios magnetic clouds, and their results are summarized in Table I. They concluded that the mean density within these clouds

TABLE I
Dependence of ICME parameters on heliocentric distance R (AU)

	BS98[a]	This work	L05[b]	W05[c]
R (AU)	0.3–1.0	0.3–1.0	0.3–5.4	0.3–5.4
S (AU)	$0.24R^{0.78}$	$0.31R^{0.53}$	$0.25R^{0.92}$	$0.19R^{0.61}$
n (cm^{-3})	$6.47R^{-2.4}$	$7.03R^{-2.18}$	$6.16R^{-2.32}$	$6.7R^{-2.4}$
V (km/s)		$483R^{0.07}$	$458R^{0.002}$	$456R^{-0.003}$
T (10^3 K)		$44.3R^{-0.83}$	$35.4R^{-0.32}$	$29.2R^{-0.74}$
Mean B (nT)	$17.7R^{-1.73}$[d]	$10.3R^{-1.31}$	$7.35R^{-1.40}$	$8.3R^{-1.52}$
V_{ex}		$39.7R^{-0.16}$	$57.5R^{-0.12}$	$0.12V_{\rm ICME}R^{-0.39}$
γ_p			1.14 ± 0.03	

[a]Bothmer and Schwenn (1998) magnetic clouds.
[b]Liu *et al*. (2005).
[c]Wang *et al*. (2005).
[d]Axial magnetic field (M. Leitner, personal communication, 2004).

decreased with heliocentric distance slightly faster than the $n = 6.1R^{-2.1}$ cm^{-3} variation found by Helios generally in the solar wind (Schwenn, 1990). Based on an analysis that included magnetic clouds observed by Pioneer 10 and Voyagers 1/2 beyond 1 AU, the radial size ($S = \int V_{sw}dt$ during cloud passage) was found to increase as $S = (0.24 \pm 0.01) \times R^{(0.78\pm0.1)}$ AU. Bothmer and Schwenn (1998) noted that the expected $R^{-2.56}$ mass density dependence agrees reasonably well with that observed, assuming clouds have a cylindrical cross-section, the flux-tube length is proportional to R, and mass is conserved within the flux tube. The axial magnetic fields inferred from force-free fits to these magnetic clouds declined as $B = 17.7 \times R^{-1.73}$ nT (M. Leitner, personal communication, 2004).

Figure 6 shows the radial dependence of the mean values of several parameters within an expanded sample of 103 Helios ICMEs during 1975–1980, including some non-cloud events not considered by Bothmer and Schwenn (1998) (e.g., Cane *et al*., 1997). The results are also summarized in Table I together with those of the recent papers of Liu *et al*. (2005) and Wang *et al*. (2005), which include both Helios and Pioneer Venus Orbiter (PVO) observations within the inner heliosphere and Ulysses observations out to 5.4 AU. Their results refer to "ICME-like" structures identified primarily using the abnormally low proton temperature signature.

All these studies show that ICMEs expand with heliocentric distance, though the dependence varies from $\sim R^{0.5}$ to $R^{0.9}$. The average size at 1 AU is $\sim$ 0.25 AU. The radial dependences in ICME plasma density are in good agreement ($\sim R^{-2.3}$), and again the density declines only slightly faster than in the general solar wind at Helios (as also found by González-Esparza *et al*. (1998) in ICMEs beyond 1 AU). The mean ICME speed has no significant radial variation ($R^{-0.003}$ to $R^{0.07}$), suggesting that, on average, there is little acceleration or deceleration between 0.3 AU and

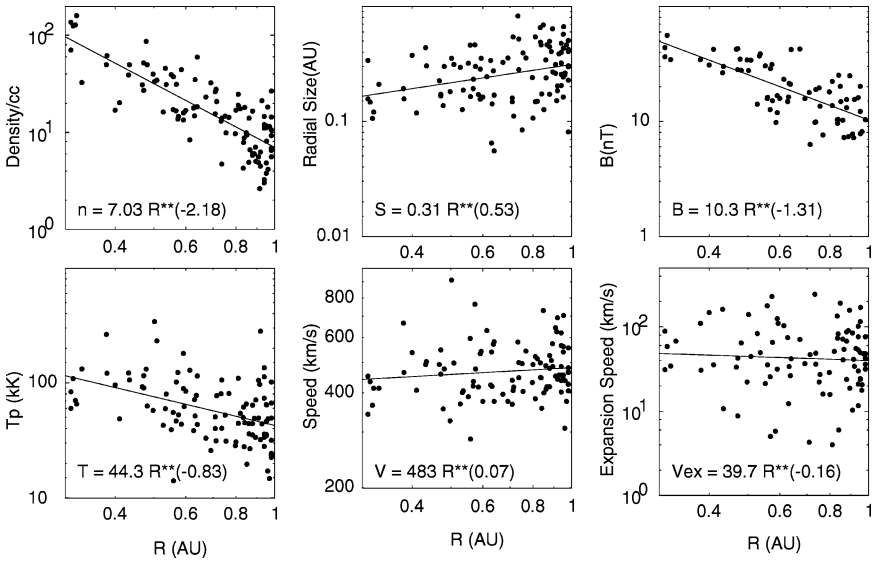

Figure 6. Variation of event-averaged ICME parameters with heliocentric distance observed by the Helios 1/2 spacecraft in 1975–1980, plotted in a log-log format.

the outer heliosphere. Mean ICME speeds are also similar to the average solar wind speed measured during the Helios missions (481 km/s; Schwenn, 1990). The proton temperature declines with distance ($R^{-0.3}$ to $R^{-0.8}$). This is comparable to, but slightly slower than the $\sim R^{-0.9}$ dependence found generally in Helios 1 solar wind data by Totten *et al.* (1995). Wang *et al.* (2005) note that this result is contrary to the expectation that adiabatic cooling due to ICME expansion will lead to faster cooling of ICME plasma. The mean magnetic field intensity declines as $\sim R^{-1.3}$ to $R^{-1.5}$. This rate of decrease is slower than for both the Parker-spiral magnetic field – relative to the Parker field, the mean field for the ICMEs in Figure 6, for example, increases as $R^{(0.44\pm0.16)}$ – and the axial fields inferred for the Bothmer and Schwenn (1998) magnetic clouds by M. Leitner (private communication, 2004). ICME expansion speeds (estimated as half the difference in solar wind speeds inside the ICME leading and trailing edges) have no significant radial dependence. Average values ($\sim$ 40–60 km/s) are around half the Alfvén speed in the ICME ($V_A \sim 85R^{-0.2}$ km/s for average values of the field and density for the ICMEs in Figure 6) as previously noted by Klein and Burlaga (1982). Liu *et al.* (2005) estimate the proton polytropic index (γ_p) to be 1.14. Totten *et al.* (1995) note that the radial dependencies in the solar wind density ($n \propto R^{-\beta}$) and proton temperature ($T \propto R^{-\delta}$) are related to the proton polytropic index by $\gamma = 1 + \delta/\beta$, obtaining $\gamma \sim 1.46$ for the Helios solar wind observations. This is comparable to $\gamma \sim 1.38$ obtained in the same way for the ICMEs in Figure 6.

Radial variations may also be examined in individual ICMEs observed by multiple spacecraft located at similar heliolongitudes but different radial distances.

Unfortunately, such events are rare. One example was observed by Helios 2 (0.4 AU, W5°) on April 23–24, 1979, and by IMP 8 (1 AU) on April 25–26. The estimated radial dependencies ($B \sim R^{-1.07}$; $T \sim R^{-0.2}$; $n \sim R^{-1.43}$; $V \sim R^{0.07}$; and $S \sim R^{0.31}$) overall are slightly weaker, though generally not inconsistent with, those inferred from the statistical results. Russell *et al.* (2003) discuss the properties of two magnetic clouds observed both at ACE (at 1 AU) and NEAR (at ∼1.7 AU). They find that the flux rope radii vary as $R^{0.96}$ or $R^{0.84}$, consistent with the results in Table I.

3.2. ICME Speeds

Figure 6 and Table I suggest that average ICME speeds at 0.3–1 AU show little radial variation. Nevertheless, ICMEs evidently do accelerate or decelerate after leaving the Sun, since transit speeds through the inner heliosphere typically differ from, though are correlated with, measured *in-situ* speeds or the speeds of the associated CMEs at the Sun (e.g., Schwenn, 1986; Cliver *et al.*, 1990; Lindsay *et al.*, 1999). For example, Lindsay *et al.* (1999) inferred that *in-situ* speeds at ∼ 0.7–1 AU are related to the CME speed ($V_{\rm CME}$) by $V = 360 + 0.25 V_{\rm CME}$ and tend to converge to the speed of the ambient solar wind. Gopalswamy *et al.* (2000) summarized the relationship between *in-situ* and CME speeds in terms of a constant ICME acceleration (a in m/s^2) during transit to 1 AU, given by $a = 1.41 - 0.0035 V_{\rm CME}$. This implies that CMEs with speeds > (<) 405 km/s decelerate (accelerate) en route to 1 AU. (See Section 3.1 in Forbes *et al.* (2006, this volume) for a theoretical discussion of ICME speeds.)

Figure 7 shows observed travel times to 1 AU (defined by the arrival of the ICME-associated interplanetary shock) for 75 events examined by Schwenn *et al.* (2005). The solid line shows a fit to the transit times given by $T_{tr} = 203 - 20.77 \ln(V_{\rm CME})$. For comparison, the dashed line assumes propagation at a constant speed $V_{\rm CME}$. Again, the tendency for fast CMEs to decelerate, and slow CMEs to accelerate, is evident. The transit times of individual shocks, however, do show considerable scatter about the fitted line. Schwenn *et al.* (2005) discuss several factors that influence transit times. For example, CME expansion speeds measured against the plane of the sky do not necessarily correspond to speeds along the Sun-Earth line, though they are evidently correlated to some extent. In particular, Dal Lago *et al.* (2003) and Schwenn *et al.* (2005) estimate that the radial expansion speeds of CMEs are typically ∼88% of the lateral expansion speeds. Similarly, Gopalswamy *et al.* (2001a) concluded that the plane of the sky halo CME speed "seems a reasonable representation of the CME initial speed." Travel times also depend on whether the arrival time of the shock (Schwenn *et al.*, 2005), ICME material (Gopalswamy *et al.*, 2000, 2001), or first ICME-related disturbance (Cane and Richardson, 2003a) is considered. In the latter case, Cane and Richardson (2003a) estimate that mean 1 AU transit speeds range from $V_T \sim 0.4 V_{\rm CME}$ up to $V_T \sim 400 + 0.8 V_{\rm CME}$, implying transit times of ∼1.1 to 2.9 days for a 1500 km/s CME. For comparison, the constant speed assumption gives 1.16 days and the Gopalswamy *et al.* (2000) model

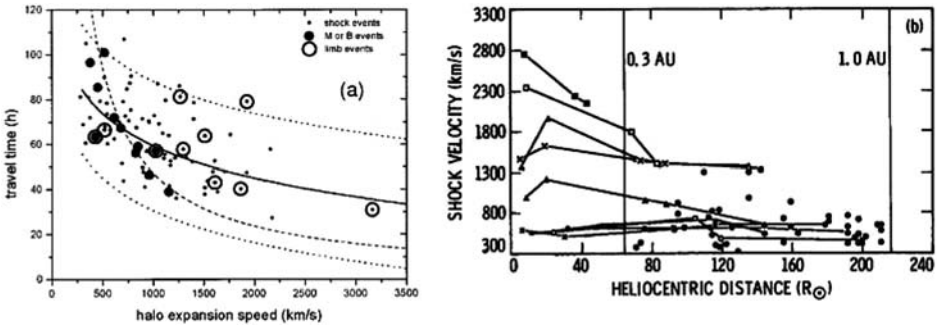

Figure 7. (a) Observed ICME-driven shock transit times vs. LASCO CME expansion speeds (Schwenn *et al*., 2005) compared with a fit to mean transit times (solid line; dotted lines indicate 2 standard deviations from fit) and assuming constant speed (dashed line). Large solid dots indicate ICME transit times for events without upstream shocks that are not included in the fit. (b) Shock speeds vs. heliocentric distance measured in situ at Helios 1/2 (•) and by radio Doppler scintillation observations (lines; heavy lines = associated with strong flares) (Woo, 1988).

$\sim$1.4 days for the time of ICME arrival. Interestingly, the Schwenn *et al*. (2005) formula gives a longer (2.1 day) mean shock transit time. Apparently this is because it is better constrained by observations of high-speed events than the Gopalswamy *et al*. (2000) model, which was only based on CMEs with speeds below 1100 km/s and converges to the constant speed assumption at high speeds. For ICMEs associated with geomagnetic storms, Zhang *et al*. (2003) estimate $T_{tr} = 96 - V_{\mathrm{CME}}/21$ hours, though this formula evidently cannot be applied to exceptionally fast CMEs, since $T_{tr} \rightarrow 0$ as $V_{\mathrm{CME}} \rightarrow 2016$ km/s. In summary, it is arguable whether methods based on halo CME speeds can give reasonably reliable forecasts of ICME or shock arrival times for space weather purposes, given the large scatter in transit speeds for similar CME speeds (e.g., Cane and Richardson, 2003b; Schwenn *et al*., 2005).

3.3. SHOCKS

Several types of observations provide information on the propagation of ICME-driven shocks in the inner heliosphere. The tracking of shocks via type II radio emissions is discussed in Section 5. Shock speeds have been measured in situ by the Helios spacecraft at 0.3 to 1 AU (e.g., Sheeley *et al*., 1985). Within the unexplored region between the Sun and the orbits of the Helios spacecraft, shock speeds may be inferred from coronagraph CME observations and by Doppler scintillation measurements of spacecraft radio signals along sight lines passing close to the Sun. Combining the latter measurements with Helios observations (e.g., Woo, 1988; Woo and Schwenn, 1991) suggests that shocks generally decelerate before reaching Helios, as shown in Figure 7(b). In particular, shocks associated with strong flares (heavy curves) show high initial speeds and rapid deceleration near the Sun. Using CME and Helios observations, Cane *et al*. (1986) concluded that relatively

slower shocks result from CMEs associated with filament eruptions accompanied by weak X-ray and microwave bursts. Typically, slower shocks near the Sun show less variation in speed with heliocentric distance.

3.4. Waves, Turbulence and Discontinuities Within ICMEs

The solar wind is pervaded by waves and turbulence on a wide range of scales (see, for example, Marsch (1991) for a comprehensive review). An active turbulent cascade transfers energy from large-scale waves (time scales of hours in the spacecraft frame) which originate in the corona and dissipates it at kinetic scales by heating the plasma. The waves and turbulence can be detected as broadband fluctuations in the magnetic field and plasma velocity and density. The turbulent cascade is less developed in high-speed wind from coronal holes than in slow wind, and power levels tend to be higher in fast wind. These differences probably result from the different conditions in the corona where fast and slow wind streams originate. There are also large numbers of sharp changes in magnetic field direction (discontinuities), many of which are tangential (Knetter *et al*., 2004), having no magnetic field threading through the plane of the structure.

It has long been known that the amplitude of fluctuations within ICMEs tends to be considerably lower than in the ambient solar wind (Zurbuchen and Richardson, 2006, this volume). However, there have been few detailed studies of the nature of fluctuations within ICMEs. Ruzmaikin *et al*. (1997) compared the spectral index of fluctuations in fast solar wind, slow wind and within ICMEs. They found that fluctuations in ICMEs were statistically similar to those in slow wind, but not to those in fast wind. They argued that the nature of the fluctuations depends on conditions in the corona where the solar wind originates and therefore that solar wind in slow streams and ICMEs probably originates in similar, most likely closed magnetic field regions in the corona.

Leamon *et al*. (1998) considered the "geometry" of the fluctuations – that is, whether turbulent energy was largely in wave vectors parallel or perpendicular to the magnetic field direction – within and around a magnetic cloud, in both the inertial range of the turbulent cascade and the dissipation scales. While the results were complicated and rather difficult to interpret, they, like those of Ruzmaikin *et al*. (1997), are consistent with turbulence in ICMEs being more like the dynamically old fluctuations in slow wind than fluctuations in fast wind.

In contrast to the low level of magnetic field and plasma variability within magnetic clouds, the sheath of solar wind plasma upstream of fast ICMEs tends to contain large-amplitude fluctuations as a result of being compressed and shocked by the ICME. These enhanced fluctuations may produce large negative values of the GSM Z component of the magnetic field, which, when combined with the increased density in the compressed sheath, can make these regions highly geoeffective (Crooker, 2000; see also Figure 1 of Zurbuchen and Richardson, 2006, this volume).

Vasquez *et al*. (2001) performed a detailed study of discontinuities within an ICME which contained multiple ejecta and showed that there were many tangential discontinuities within the boundaries between the ejecta. Such discontinuities are interesting not only in terms of the large-scale structure of ICMEs – since they form topological boundaries between different plasma regions – but also because energetic particle diffusion coefficients are much lower in their presence. Discontinuities are also important in the upstream sheath region: Intriligator *et al*. (2001) argued that discontinuities dramatically reduced particle diffusion across corotating interaction regions. A similar effect should be present within ICME sheaths, perhaps helping to explain the effectiveness of the sheath region in cosmic ray Forbush decreases (e.g., Burlaga, 1991).

4. ICME Dynamics and Interactions

I. G. RICHARDSON, N. U. CROOKER, D. ODSTRCIL AND J. M. SCHMIDT

4.1. ICME-STREAM AND ICME-ICME INTERACTIONS

The ambient solar wind through which ICMEs propagate is divided into intervals of slow ($\lesssim$400 km/s) solar wind and faster flows emerging from coronal holes which produce a quasi-stationary pattern that corotates with the Sun. Regions of compressed plasma (corotating interaction regions, CIRs) form at the leading edges of high-speed streams as they collide with the preceding slower solar wind (for a comprehensive review see the ISSI volume by Balogh *et al*., 1999). One effect of high-speed streams on ICMEs is that, since ICME speeds tend to converge to the ambient solar wind speed, ICME travel speeds may be higher when propagating through high-speed streams. However, ICMEs are only infrequently embedded in high-speed flows, presumably because ICME sources rarely if ever lie in the weak field regions underlying coronal holes. For example, only $\sim$8% of the ICMEs identified by Cane and Richardson (2003a) at 1 AU arrived during passage of a high-speed stream. A few examples have been observed by Ulysses within high-speed flows above polar coronal holes (e.g., Gosling *et al*., 1998) although these may have expanded into the fast wind from adjacent high-field sources rather than directly from coronal hole sources (e.g., Hammond *et al*., 1995). More frequently, ICMEs are found near high-speed stream leading edges or in slow, interstream solar wind. These typically overlie the solar active regions and meandering solar neutral line from which CMEs arise (e.g., Crooker and Cliver, 1994). A particularly interesting situation occurs when the ICME forms the slower-speed plasma immediately preceding the fast stream. Plasma within the trailing edge of the ICME may be compressed in this situation, and, if the embedded magnetic field is directed southward, enhancement of the southward field by compression may lead to stronger geomagnetic effects than would have occurred in the absence of the interaction with the

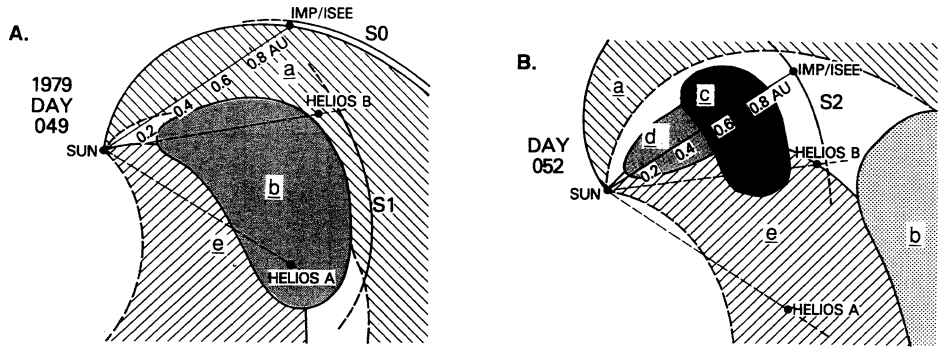

Figure 8. Sketch of an evolving complex stream in February, 1979 (Behannon *et al.*, 1991).

fast stream (e.g., Zhao, 1992; Cane and Richardson, 1997; Fenrich and Luhmann, 1998; Crooker, 2000).

Interactions between more than one ICME may occur, in particular at times of elevated solar activity levels. Figure 2(c) of Zurbuchen and Richardson (2006, this volume) illustrates two aspects of such interactions. First, the ICME shown apparently consists of two components, which suggests that the ICME may have been formed by the interaction of two individual ICMEs. Second, the associated shock is traveling through plasma associated with a preceding ICME, as indicated, for example by depressed proton temperatures and enhanced Fe charge states, rather than ambient solar wind. For further discussion of ICME-ICME interactions and boundaries within ICMEs, see (Wimmer-Schweingruber *et al.*, 2006, this volume).

Burlaga (1975) pointed out that many high-speed flows are contiguous but composed of multiple components, either streams or ICMEs, applying the term "compound streams" to such regions. Figure 8 shows a sketch of a complex, evolving compound stream inferred from observations by the Helios and near-Earth spacecraft and interplanetary scintillation data (Behannon *et al.*, 1991). Structures "a" and "e" are corotating high-speed streams, while "b" to "d" are transient structures.

4.2. Interplanetary Reconnection

Field lines on the surface of a CME with the structure of a magnetic flux tube propagating within the radial magnetic field near the Sun can reconnect with the external magnetic field if oppositely-directed magnetic field lines are squeezed together due to the flux tube motion (e.g., McComas *et al.*, 1994; Moldwin *et al.*, 1995; Rogers *et al.*, 2000). Figure 9 (Schmidt, 2000; Schmidt and Cargill, 2003) shows a flux tube with field lines rotating in an anticlockwise sense, projected onto the plane in which the x-axis is in the ecliptic plane and the z-axis is parallel to the solar rotation axis. An outward-directed, distorted, radial solar magnetic field is assumed in the northern hemisphere and an inward-directed field in the southern hemisphere, separated by a current sheet in the ecliptic plane. Due to the sense

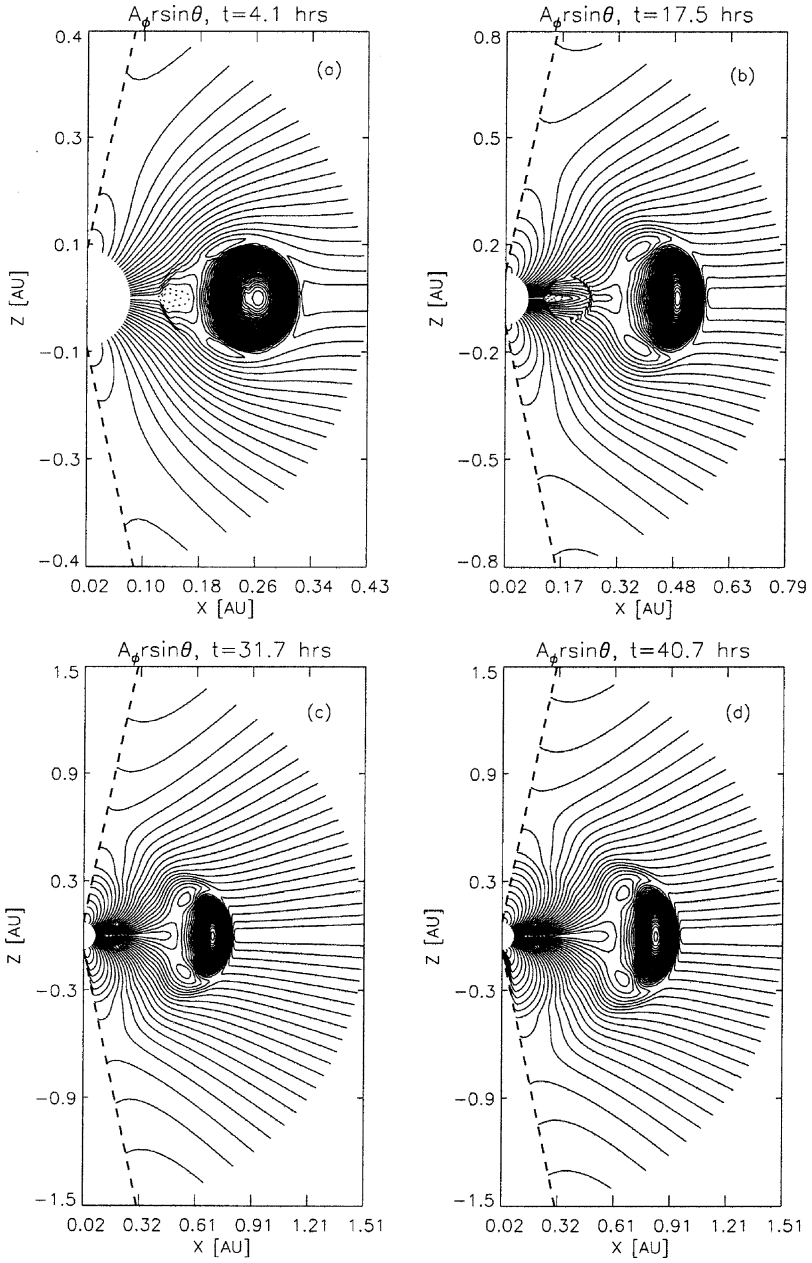

Figure 9. A magnetic flux tube propagating initially at 1.5 times the solar wind speed in a current sheet. Reconnection regions develop that are symmetric with respect to the ecliptic plane (Schmidt, 2000; Schmidt and Cargill, 2003).

of rotation of the flux tube magnetic field, reconnection occurs at the northern and southern leading edges of the tube symmetrically about the ecliptic plane. When the flux-tube reaches about 1 AU (after 40.7 hours), reconnection has reduced its size by almost one third. An equivalent fraction of the internal material, when released from the flux tube, contributes to local heating and momentum transfer to the solar wind plasma. Reconnection becomes more effective as the flux tube speed and field strength increase relative to their values in the solar wind. When the magnetic field of the flux tube is as weak as the external field, the tube completely loses its magnetic form by the time it reaches Earth's orbit.

4.3. Modeling ICME Propagation in a Structured Medium

Numerical simulations provide an important tool for understanding ICME interactions with the ambient medium. Two and a half-D MHD simulations have shown significant distortions of the shock front when propagating along the heliospheric current sheet (Odstrcil *et al.*, 1996; Hu, 1998). Simulations with a 2-D hydrodynamic model have demonstrated that the parts of a single ICME straddling both high- and low-speed flows would evolve radically differently in the two regions (Riley *et al.*, 1997). The 3-D interactions between transient and corotating structures produce a rich set of dynamic phenomena. A single interplanetary disturbance can have radically different appearances at various locations. The appearance also depends critically upon the CME launch location with respect to the streamer belt flow (Odstrcil and Pizzo, 1999a,b).

An example of a model CME flux tube propagating through a structured solar wind is shown in Figure 10 (Schmidt and Cargill, 2001). The flux tube is initially in slow, low-latitude solar wind with speeds of about 300 km/s. It is then given an initial negative meridional velocity that drives it into higher-latitude, high-speed (600 km/s) solar wind (the division between the low- and high-speed wind is at 45° latitude). The first two panels of Figure 10 show that the penetration of the

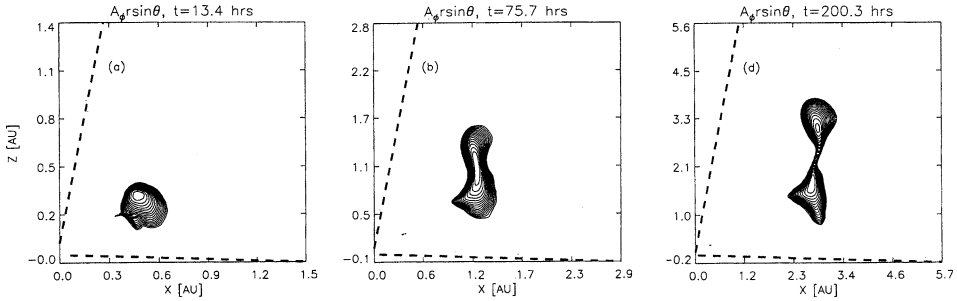

Figure 10. The evolution of a magnetic flux tube initially located in slow, low-latitude, solar wind that is given an initial meridional velocity (−300 km/s) that takes it into the region of high-latitude, high-speed wind (Schmidt and Cargill, 2001). The tube is projected onto the plane defined by the in-ecliptic x-axis and rotation axis of the Sun z.

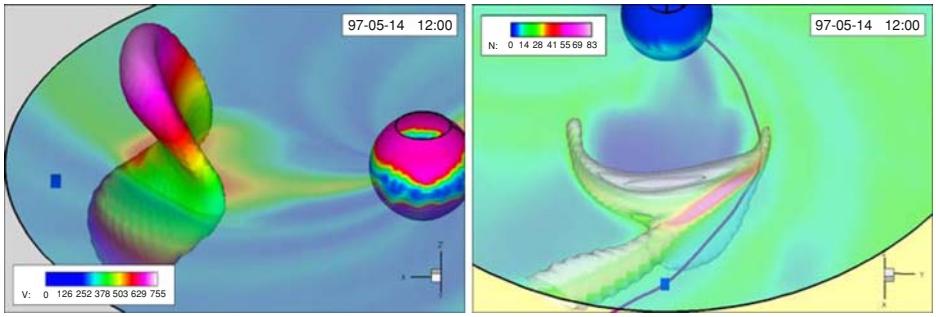

Figure 11. Numerical simulation of ICME associated with the 12 May 1997 solar event (adapted from Odstrcil *et al*., 2004).

flux tube into the high-speed wind is very slow. This is because an additional $\mathbf{j} \times \mathbf{B}$ force acts on the tube when it enters the high-speed wind, opposing its motion. As soon as the tube crosses the boundary, however, a portion begins to pull away in the high-speed wind, although it never completely separates owing to magnetic tension forces along a corridor of linking field lines. In addition, the flux tube stretches meridionally because pressure gradients are smaller in the meridional than in the radial direction.

Odstrcil *et al*. (2004) found that even relatively small-scale structures in the background solar wind may play an important role in the interplanetary evolution of transient disturbances. Figure 11 shows a numerical simulation of the ICME associated with the 12 May 1997 solar event injected into a structured solar wind. In the left-hand panel the colour scale indicates flow speed, the translucent plane represents the equatorial plane, and the injected ICME is indicated by the iso-surface at 6 cm^{-3}. The position of Earth is shown by the blue box. In the right-hand panel, the color scale indicates plasma density. The density structure defined by a white iso-surface at 30 cm^{-3} outlines both the compressed ICME structure and a corotating interaction region (CIR) threaded by a magnetic field line (blue). The results show that: (a) injected material undergoes substantial latitudinal distortion caused by the large-scale, bi-modal velocity structure of the background solar wind; and (b) an interplanetary shock formed in the slow streamer belt is modified when it merges with the CIR caused by fast flow from an equatorward extension of the southern coronal hole. These effects can be observed by *in-situ* and remote white-light observations (see Section 6, Figures 13 and 14).

5. Solar Cycle Variations

I. G. RICHARDSON

The occurrence rate of ICMEs essentially follows the ∼11-year solar activity cycle (e.g., Lindsay *et al*., 1994; Cane and Richardson, 2003a). This was evident

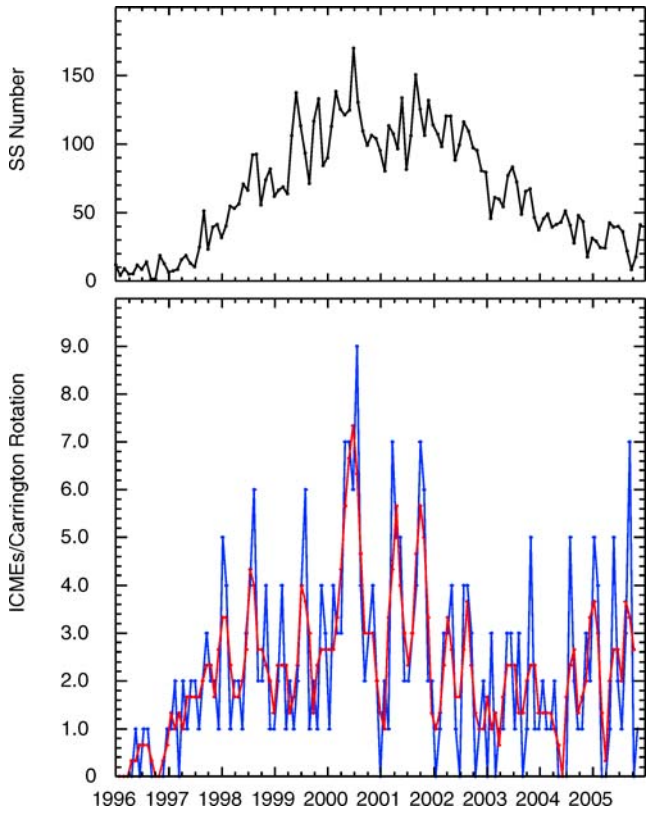

Figure 12. Monthly sunspot number in 1996–2005 (upper panel) together with the ICME rate/Carrington rotation (plus 3-rotation running means) at 1 AU, updated from Cane and Richardson (2003a).

indirectly even before the space era, for example, from the rate of "sporadic" geomagnetic storms, now known to be predominantly associated with ICMEs and their related shocks (e.g., Gosling *et al.*, 1991; Cliver, 1995; Richardson *et al.*, 2001 and references therein). Several studies have tracked the occurrence rate of various ICME signatures throughout the solar cycle. For example, Gosling *et al.* (1992) noted that bi-directional suprathermal electron strahls were observed in $\sim$1% of the near-Earth solar wind at solar minimum, rising to $\sim$15% around solar maximum, when $\sim$4 events/month were identified (Gosling, 1990). Figure 12 shows the ICME rate/solar rotation (plus 3-rotation running averages) in the near-Earth solar wind estimated by Cane and Richardson (2003a) since 1996 and updated/revised to the end of 2005. The ICMEs are identified principally from examination of the solar wind plasma and magnetic field observations. Note that the rate increased by an order of magnitude from $\sim$0.3 ICMEs/rotation in 1996 to $\sim$3/rotation in 1998–2002, though with several brief intervals with higher rates during this time that are associated with periods of exceptionally high solar activity. Interestingly,

these variations are quasi-periodic with a dominant period of ∼166 days (Cane and Richardson, 2003a; Richardson and Cane, 2005), similar to the "154-day" periodicity intermittently present in various solar and interplanetary phenomena during cycle 23 and earlier solar cycles (e.g., Cane *et al*., 1998; Dalla *et al*., 2001, and references therein). The sunspot number is also shown, illustrating that there is no simple correlation between solar activity levels and the ICME rate, such as that between solar activity and the CME rate reported by Webb and Howard (1994) (see, also, Schwenn *et al*., 2006, this volume). In particular, there was a temporary decline in the ICME rate in 1999, yet solar activity continued to increase. Furthermore, the ICME rate has remained relatively high in 2004–2005 (with occasional brief intervals of higher rates due to bursts of enhanced solar activity) despite the substantial decline in sunspot number (Richardson and Cane, 2005).

Given that an ICME takes ∼1 day to pass a spacecraft, it is clear from the occurrence rates in Figure 12 that even at solar maximum, ICMEs generally do not dominate the near-Earth solar wind, except possibly during brief periods of exceptionally high solar activity. For example, on average, the Cane and Richardson (2003a) ICMEs were observed for ∼1% of the time during 1996, increasing to ∼16% in 2000–2001 (cf. Gosling *et al*., 1992). Typically at solar maximum, the near-ecliptic solar wind at ∼1 AU is approximately equally divided between (a) ICMEs and the associated post-shock flows; (b) fast streams from coronal holes, and (c) slow, interstream solar wind (Richardson *et al*., 2002). Furthermore, although ICMEs tend to have stronger than average magnetic field strengths, ICMEs typically do not dominate mean interplanetary magnetic field strengths at solar maximum. In particular, fields carried by ICMEs do not appear to be responsible for the increase in mean IMF strength as activity levels increase because this increase is present in the ambient solar wind, outside of ICMEs (Richardson *et al*., 2002). Smith and Phillips (1997) estimate that removing ICMEs would decrease the average IMF by only ∼8%. On the other hand, Crooker *et al*. (2004) suggest that the "legs" of ICMEs whose leading edges have passed far out into the heliosphere may contribute to the increase in mean IMF strength and may be difficult to distinguish from ambient solar wind.

During brief intervals of unusually high solar activity, it is possible that the ICMEs interact with themselves and other solar wind structures, such as CIRs, to form so-called "global merged interaction regions" (GMIR)s. These shell-like structures with intense magnetic fields that encircle the Sun and extend to fairly high latitudes have been suggested as the cause of step-like decreases in the long-term (11-year) modulation of galactic cosmic rays (Burlaga, 1995, and references therein). See Gazis *et al*. (2006, this volume) for further discussion of GMIRs. In addition, Cliver and Ling (2001) and Cliver *et al*. (2003) have argued that ICMEs, in particular the strong magnetic fields in the "tail" of the field distribution that are predominantly associated with ICMEs, drive long-term modulation. However, the role of ICMEs in long-term modulation (cf. Gazis *et al*., 2006, this volume) is still a topic of debate – see, e.g., Wibberenz *et al*. (2002) for an alternative viewpoint.

6. Comparison of Observations and Models

D. ODSTRCIL, C. CID, J. A. LINKER AND J. M. SCHMIDT

Efforts to date have been devoted mainly toward increasing the sophistication of numerical models and to improving understanding of ambient and transient disturbances. Relatively few papers have been published on the numerical simulation of observed events. This is due mostly to the inherent difficulties of such a task and by the lack of reliable observational data to initialize the numerical models. Nevertheless, such activities are vital for supporting the analysis of various *in-situ* and remote observations and for the development of space weather forecasting capabilities. This section describes recent achievements in numerical modeling of specific heliospheric events.

6.1. MODELING A CME FROM SUN TO EARTH

The simplest models are empirical, with the aim being to predict the arrival of CMEs at Earth (Gopalswamy *et al.*, 2001a; Schwenn *et al.*, 2005). More sophisticated numerical MHD models have the potential to predict the solar wind density, mean temperature, and components of the flow velocity and magnetic field. A successful match with observations requires not only an adequate physical model and numerical resolution but also reliable observations to drive the computations. Note that both ambient solar wind and transient disturbances have to be well-replicated in the modeling process, since their 3-D interactions can significantly modify their structure en route to Earth.

Significant progress has been made in simulating the ambient solar wind (Linker *et al.*, 1999; Usmanov *et al.*, 2000; Riley *et al.*, 2001; Arge *et al.*, 2002; Hayashi *et al.*, 2003; Roussev *et al.*, 2003). The simulation of 3-D transient disturbances is less mature, and various models have been used to emulate the CME launch and propagation (Detman *et al.*, 1991; Odstrcil and Pizzo, 1999a; Groth *et al.*, 2000; Vandas *et al.*, 2002; Odstrcil *et al.*, 2004; Manchester *et al.*, 2004a; Roussev *et al.*, 2004). This section reviews three case studies.

12 MAY 1997 EVENT

The 12 May 1997 halo-CME event has been chosen for detailed studies by the scientific community (`http://solarmuri.ssl.berkeley.edu`, `http://www.bu.edu/cism`, `http://www.shineorg.org`). Solar and heliospheric background conditions at that time were relatively simple, thereby facilitating analysis and modeling. However, because the photospheric vector magnetograms for that period are unfortunately of low quality, self-consistent "data-driven" simulation of the solar eruption has proven to be unusually challenging (Z. Mikic, private communication). As a consequence, "data-inspired" simulations have been

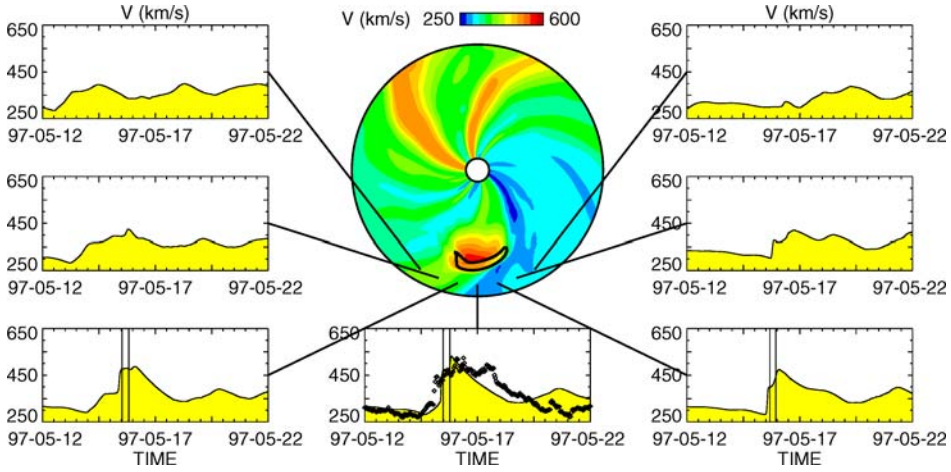

Figure 13. Simulated multi-point *in-situ* observations of a transient disturbance at different positions in the equatorial plane at 1 AU (Odstrcil *et al*., 2005). The central top image shows the solar wind radial velocity in the equatorial plane on 15 May 1997 at 00:00 UT. The seven plots show the temporal evolution of the solar wind radial velocity at the different observing positions as indicated by solid lines. The vertical lines indicate the extent of the simulated ICME material, and black dots show Wind spacecraft observations at Earth.

realized (Odstrcil *et al*., 2004, 2005) to analyze this event, to provide global context, and to set a benchmark for further modeling. In these 3-D MHD simulations, the background solar wind was determined from the SAIC (Riley *et al*., 2001) or WSA (Arge *et al*., 2002) coronal model, and the transient disturbance was determined from the cone model (Zhao *et al*., 2002).

Numerical results show that the 12 May 1997 ICME interacts with the leading edge of a fast stream (see Figure 11 in Section 4.3). This results in a substantial latitudinal distortion of the injected material, a strong density compression within the heliospheric streamer belt, merging of an interplanetary shock with the CIR, and modification of the magnetic connectivity. Figure 13 shows the temporal evolution of the solar wind velocity at various positions at 1 AU. Comparison with Wind observations (plot in the middle of the bottom row) shows that it is becoming feasible to reproduce the parameters of the ambient solar wind and to estimate the arrival of interplanetary shocks and coronal ejecta. The shock stand-off distance from the driving ejecta and the shock front inclination are difficult to match because even relatively small-scale solar wind structures can significantly affect the appearance of transient disturbances. Additional work is necessary to specify smaller-scale structures, more accurate locations, and the temporal evolution of the streamer boundaries in the corona (Odstrcil *et al*., 2005). Figure 14 shows synthetic images of the white light scattered by the solar wind density structures. Such images, which show a large latitudinal distortion of the ICME with localized bright spots at the

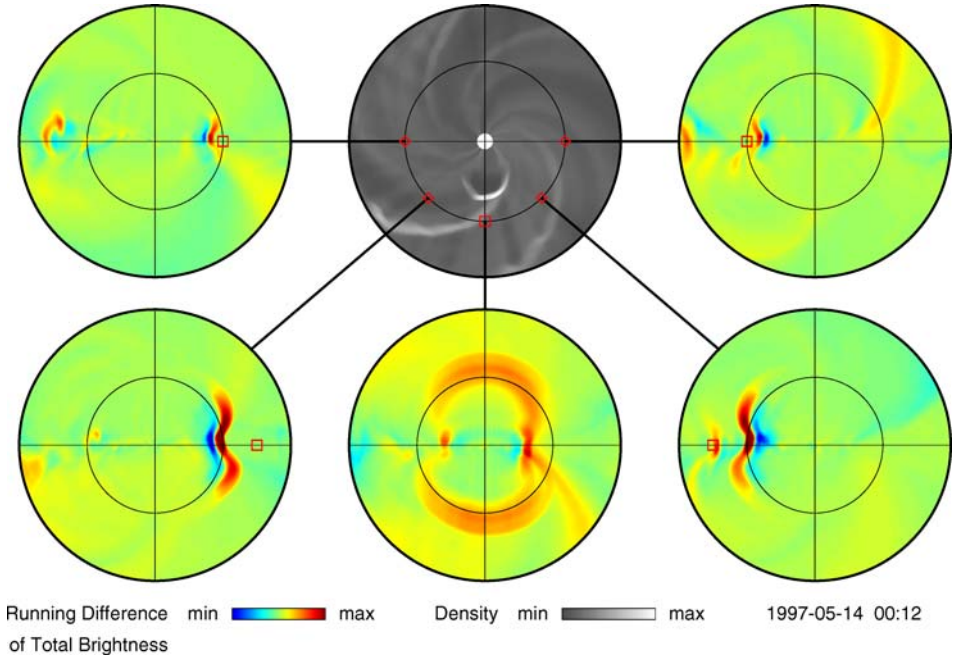

Figure 14. Simulated multi-perspective remote white-light observations of a transient disturbance from various positions in the equatorial plane at 1 AU. The central top image shows the distribution of the solar wind density scaled by $(R_A/r)^2$ in the equatorial plane on 14 May 1997 at 12:00 UT. The remaining five images show synthetic difference images of the total brightness (generated at 12:00 and 06:00 UT on May 14) as viewed from the respective observing positions indicated by solid lines. The Earth position is shown by a red square.

slow streamer, may be compared with SMEI and upcoming STEREO observations from missions with global imaging capabilities.

1–2 MAY 1998 EVENTS

The 1–2 May 1998 CME events have also been chosen for detailed studies by the scientific community (`http://solarmuri.ssl.berkeley.edu`, `http://csem.engin.umich.edu`, `http://www.shineorg.org`). These events are more complex than the 12 May 1997 event; however, the availability of high-quality vector magnetograms favors the initialization of simulations ab-initio. The University of Michigan team has recently simulated these events by the BATS-R-US code with two different initiation models. Both models start by deriving an ambient state of the global corona and solar wind from synoptic magnetograms observed by the Wilcox Solar Observatory.

In the model of the 1 May 1998 CME (Manchester *et al.*, 2004b), a Gibson-Low magnetic flux rope (Gibson and Low, 1998) is placed in the helmet streamer of the pre-event active region. Initially the flux rope is in a state of force imbalance and

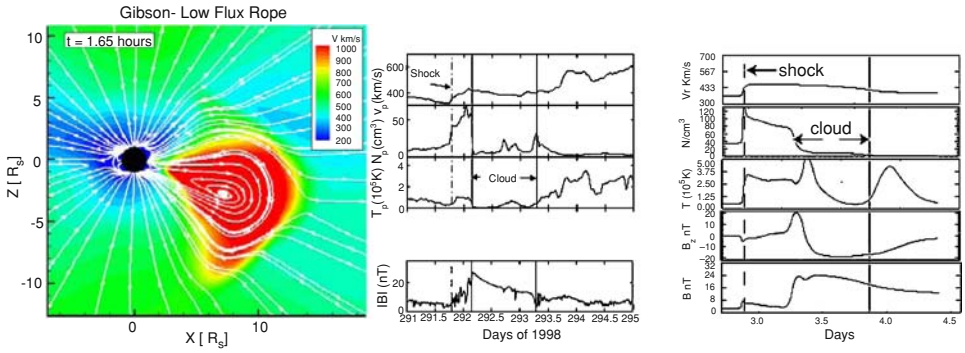

Figure 15. Simulated CME in the meridional plane (*left*) and temporal evolution of plasma parameters at Earth (*right*). The CME is shown 1.65 hours after initiation; the color scale represents the flow velocity, and white lines show the projected magnetic field lines. Observed (*left*) and simulated (*right*) temporal profiles show, from top to bottom, the radial velocity, proton number density, temperature, magnetic field southward component B_z and magnitude (adapted from Manchester *et al.*, 2004b).

expands at a rate approximating the observed speed. The bow shock ahead of the flux rope as well as the current sheet behind it are well-resolved. Figure 15 shows the magnetic field disturbed by the ICME and a comparison of plasma parameters at Earth with observations.

In the model of the 2 May 1998 CME (Roussev *et al.*, 2004), the solar eruption is initiated by slowly evolving the boundary condition for the horizontal magnetic field at the Sun until a critical point is reached where the configuration loses equilibrium. At this point the field erupts, and a flux rope is ejected with a maximum speed in excess of 1000 km/s. A shock forms in front of the flux rope, and it reached a fast-mode Mach number in excess of 4 at $5R_S$. Diffusive-shock-acceleration theory predicts a distribution of solar energetic protons with a cut-off energy of about 10 GeV (Roussev *et al.*, 2004; Forbes *et al.*, 2006, this volume).

6.2. Multiple Events

On 10 June 2000 between 16:30 and 19:30 UT, the Wind/WAVES instrument detected an extremely narrow-band radio type-II burst which was flanked by intense radio type-III bursts (Gopalswamy *et al.*, 2001b). That event was associated with the collision of a slow, dense CME with a fast, less dense CME approaching from behind, as can be seen in the LASCO coronagraph images (inverted, see caption) in Figure 16.

Although not all CME collision events are so intense that they can give rise to a radio signal burst (e.g., Richardson *et al.*, 2003), it has been argued that there is a strong correlation with such events (e.g., Gopalswamy *et al.*, 2001b, 2002). The top panels of Figure 16 show results from a simulation of the observed collision event. The simulation box, indicated by the thick dashed lines, comprises the field of view of the C2 and C3 LASCO coronagraphs, and the geometrical dimensions

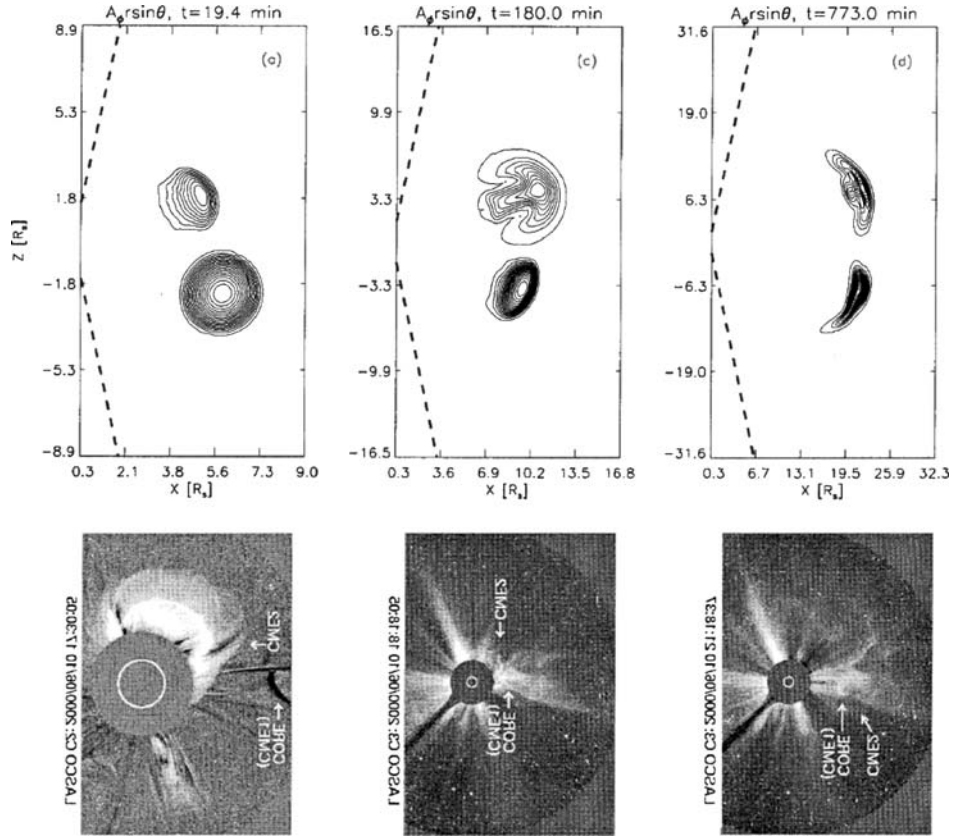

Figure 16. Contour plots (top panels) of the vector potential at three times during the evolution of a shock interaction between two colliding CMEs which are separated by a meridional angle of 40°. The plots model the 10 June 2000 events in the LASCO images (bottom panels), which have been inverted to match. They show that the fast CME2 catches up with the slow CME1 (first panel), that CME1 is deflected and flattened by the shock driven by CME2 (second panel), and that CME2 and CME1 then propagate outward together (third panel) (adapted from Schmidt and Cargill, 2004; Gopalswamy *et al*., 2001b).

and velocities of the CMEs are taken from the coronagraph observations. We see that the fast, less dense (upper) CME overtakes the slow, dense (lower) CME and that the slow CME is deflected into the southern hemisphere due to an interaction with the forward shock created by the fast CME. The shock hits the slow CME along its northern edge. This impact flattens the slow CME at that location, and the shock, when it penetrates into the denser material of the slow CME, steepens significantly due to the reduced Alfvèn speed there. We find that the steepened shock persists for a long time. This circumstance favors strong acceleration of particles, provided there is an adequate population of seed particles in the ambient plasma.

7. Remote Sensing of ICMEs

7.1. Remote Radio Sensing and Tracking of ICMEs

M. J. Reiner

Type II radio emissions are remote signatures of coronal and interplanetary shocks (see Pick *et al.*, 2006, this volume) that are generated at the plasma frequency and its harmonic, implying that the observed frequency is directly related to the plasma density in the source region ($f_p(\mathrm{kHz}) = 9\sqrt{n_p(\mathrm{cm}^{-3})}$). It was noted that coronal (metric) type II radio bursts, generated by coronal shocks, were often associated with the occurrence of sudden commencement geomagnetic storms on Earth. This led to speculation that these coronal shocks likely extended into interplanetary space, where, due to the falloff of the plasma density with distance, they might generate radio emissions at low frequencies, below that of Earth's ionospheric cutoff at about 20 MHz. The first clear detection of a low-frequency type II burst, at kilometric wavelengths, was made by the spaceborne radio receivers on the IMP-6 spacecraft (Malitson *et al.*, 1973).

Subsequently, with better radio instrumentation on the ISEE-3 spacecraft, Cane *et al.* (1982) and Lengyel-Frey *et al.* (1989) studied the observational characteristics of these kilometric type II emissions. The example shown in Figure 17 is characterized by broad diffuse emissions that drift in frequency from ~1 MHz at 07:00 UT to 200 kHz by 10:00 UT. The smooth diffuse nature of this radiation suggests that it was generated at the harmonic of the plasma frequency (Lengyel-Frey *et al.*, 1985).

These type II radio emissions are generated by electrons accelerated at shocks. The observation of the fundamental/harmonic structure of these emissions confirmed their generation by the plasma emission mechanism (Lengyel-Frey *et al.*, 1985). While the precise physical origin of the coronal shocks that generate the metric type II bursts is not yet firmly established (see Pick *et al.*, 2006, this volume), the kilometric type II bursts observed in the interplanetary medium are unambiguously associated with CME-driven shocks (Cane *et al.*, 1987). *In-situ* observations have established that the type II radiation is generated in the upstream region of the CME-driven shock (Hoang *et al.*, 1992) by processes similar to those that generate radio emissions in Earth's electron foreshock (Bale *et al.*, 1999; Knock *et al.*, 2001).

Kilometric type II radio emissions often extend as low as 20 or 30 kHz, corresponding to plasma densities from 5 to 10 cm^{-3}, which are typical of the densities measured at 1 AU. This suggests that the radio-producing CME-driven shocks extend well into interplanetary space and that the frequency drift rate of the associated type II emissions can therefore be used to track these CME/shocks through the interplanetary medium, beyond the limit of the white-light coronagraph observations (see Schwenn *et al.*, 2006, this volume). To facilitate this interplanetary tracking, Reiner *et al.* (1997, 1998) displayed the radio dynamic spectrum as the inverse of

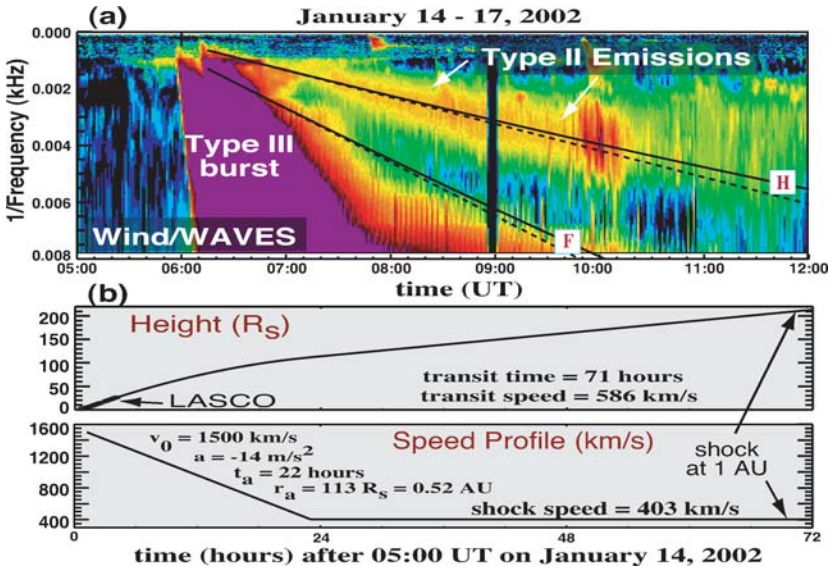

Figure 17. (a) Dynamic radio spectrum (plot of intensity as a function of inverse frequency and time) showing frequency drifting type II radio emissions for an event on January 14, 2002. On this plot a straight (dashed) line corresponds to radio emissions generated by a shock propagating at a constant speed. The solid curves correspond to type II radio emissions generated by a shock that is decelerating at a constant rate of 14 m/s^2. (b) Speed profile and height-time dependence derived from the *in-situ* and radio data for a shock propagating through the interplanetary medium in 71 hours and arriving at 1 AU at a speed of 400 km/s, as described in the text (adapted from Reiner *et al*., 2003).

the frequency versus time, as in Figure 17. Since the interplanetary density falls off as $1/R^2$ (R is the heliocentric distance), the inverse of the frequency is proportional to R. Thus, in this representation a CME/shock propagating at a constant speed will produce frequency drifting type II emissions that lie along a straight line, originating from the solar liftoff time. Deviations from a straight line may indicate acceleration or deceleration. In Figure 17, the deviation of the frequency drift from the straight dashed line indicates that the associated shock was decelerating through the outer corona.

Deriving the complete speed profile of a CME/shock from the type II radio data is difficult due to the complexities of the type II emissions, to its often sporadic and fragmented nature and to the unknown scale of the interplanetary density falloff in the source region. Reiner *et al*. (2001, 2003) proposed a simple model based on the typical behavior of CME/shocks deduced from the radio and white-light observations. The LASCO CME measurements indicate that when CMEs decelerate they tend to do so at an approximately constant rate. On the other hand, the radio observations indicate that far out in the interplanetary medium the CME-driven shocks propagate at an approximately constant speed (Reiner *et al*., 1999). Thus, Reiner *et al*. (2001) assumed that, in general, a CME shock in the outer corona will first decelerate at a constant rate, then propagate at a constant speed to 1 AU

(see Figure 7(b) and Woo, 1988). In this simple model, a family of speed profiles corresponding to different CME initial speeds can be deduced from the observed transit time of the CME/shock and from the speed of the shock at 1 AU, directly measured from the *in-situ* plasma parameters. Reiner *et al.* (2001) then select out of this family of speed profiles the one that gives the best fit to the frequency drift of the observed radio data. This technique was used to obtain the speed profile shown in Figure 17(b) for the type II event illustrated in Figure 17(a). For this particular type II event it was found that the best fit to the frequency drift of the type II (solid curve in Figure 17(a)) corresponded to the speed profile with an initial CME speed of 1500 km/s (which was essentially the same as the CME plane-of-sky speed). The unique solution suggested by the simultaneous fit to all these data then corresponded to the CME decelerating at a constant rate of 14 m/s^2 for 22 hours (corresponding to a propagation distance of 0.5 AU), then propagating at a constant speed of 400 km/s to 1 AU. The corresponding height-time curve is also shown in Figure 17(b).

Until now, the remote type II radio and the IPS observations described below have provided the only means of tracking the interplanetary transport of CMEs and their shocks. With the recent launch of the 'all sky' camera on SMEI (Eyles *et al.*, 2003), we have for the first time some white-light observations with which to compare these low-frequency and IPS radio observations (see, e.g., Reiner *et al.*, 2005).

7.2. IPS Observations of ICMEs

R. J. Forsyth

As discussed in the previous sections, coronagraphs provide a multitude of observational information on CMEs as they begin their journey out from the Sun, and a wealth of data is also available on ICMEs from 0.3 AU outwards from *in-situ* spacecraft observations. However, if we are trying to follow and understand the evolution of ICMEs as they propagate out from the Sun through the inner heliosphere, there is a key gap in observational information between $\sim 30 R_s$ and 0.3 AU. There has been growing use in recent years of the Interplanetary Scintillation (IPS) technique to provide remote sensing of ICMEs as they traverse this inner region.

IPS employs multiple antennas to measure the scintillation of distant astronomical radio sources, such as quasars (e.g., Hewish *et al.*, 1964), enabling information to be derived about the interplanetary medium through which the radio signals are passing. Two commonly used techniques are applied to study ICMEs. The first uses multiple radio sources to make sky maps of the level of turbulent fluctuations in the solar wind. The turbulence level in the sheath region ahead of ICMEs is found to be higher than the ambient, allowing these regions to be tracked as they propagate through the maps (e.g., Gapper *et al.*, 1982). The second technique applies a cross-correlation analysis to scintillation data of the same source from multiple observing stations to derive the speed of the solar wind in the region through which the signals pass (Armstrong and Coles, 1972). This can be used to remote sense the

transient high speed solar wind streams created by ICMEs. The radio frequencies at which the observations are made determines the distance range from the Sun which can be usefully explored. For example, the Nagoya University system (e.g., Tokumara *et al*., 2005) at 327 MHz samples the distance range from ∼0.2–0.9 AU, while the European EISCAT (ionospheric radar) system operating at ∼930 MHz can probe as close to the Sun as ∼18–30R_s (e.g., Breen *et al*., 2002). However, the EISCAT system tends to be used for IPS in relatively short campaigns when not in use for ionospheric studies. Thus while it has been successfully used in comparing the speeds of fast and slow solar wind streams close to the Sun with *in-situ* observations (e.g., Breen *et al*., 2002), it has not yet been seriously used to study an ICME propagating through the inner regions of the heliosphere. The advantage of IPS in being able to sample a wide range of distances in the gap between solar and *in-situ* observations is counterbalanced by difficulties in analysis and interpretation due to the measurement being an integration of the scintillation occurring all the way along the line of sight of the antenna.

Recent IPS investigations of ICMEs have focussed on case studies of individual events, attempting to make the link with one or the other or both of solar observations and *in-situ* observations of the events. Two studies have investigated the IPS signature of the 14 July 2000 CME associated with an X-class solar flare, the so-called "Bastille Day" event, using the Ooty radio telescope in India and the Nagoya system in Japan, both operating at 327 MHz (Manoharan *et al*., 2001; Tokumara *et al*., 2003). By tracking the zones of enhanced turbulence across sky maps, Manoharan *et al*. (2001) were able to deduce that the speed of the ICME declined slowly out to ∼100R_s and then much more rapidly beyond this distance, suggesting increased interaction with the ambient solar wind. Tokumara *et al*. (2003) were able to model the IPS observations to deduce that the interplanetary disturbance had a toroidal shape. Tokumara *et al*. (2005) identified 10 interplanetary disturbances in Nagoya IPS data during a 19 day period of intense solar activity in October-November 2003. They were able to identify an interplanetary disturbance associated with all shock events observed *in-situ* at 1 AU during this period as well as possible links to solar flare events, although not on a one-to-one basis. For two particular events it was possible to establish the full chain of events through from solar origin to *in-situ* observation. A similar end-to-end to study was made of an April 2000 event by Jadav *et al*. (2005).

8. Conclusions

In this chapter we have reported on our present-day knowledge of ICMEs in the inner heliosphere, relating observations of their origin in the solar corona to *in-situ* spacecraft observations and discussing the evolution that takes place in between.

– Attempts to relate the coronal and *in-situ* observations (Section 2) to date have focussed on the relationship between the three-part CME and the

interplanetary magnetic flux rope of the ICME. While it is still not fully clear how the different parts of the CME evolve and what signatures they lead to in the *in-situ* data, certain aspects, such as the handedness and orientation of the coronal flux rope, do appear to survive the interactions and distortions that affect the CMEs as they expand out into the heliosphere.
– Studies of the evolution of ICME parameters (Section 3) confirm that ICMEs expand as they travel out through the heliosphere and can both decelerate and accelerate compared to the speeds of the corresponding CMEs observed by coronagraphs. However, calculations of the travel time from the corona to 1 AU based on these speeds give results with a considerable scatter.
– Some of the more complex *in-situ* observations can be understood by the interaction of ICMEs with both the stream structure of the solar wind and with other ICMEs of differing speeds (Section 4). Numerical simulations have proven a valuable aid to understanding these interactions.
– Solar cycle effects are apparent in ICME occurrence rates (Section 5) and to some extent in magnetic cloud axis orientations (Section 2).
– Progress has been made in the numerical modeling and comparison to observations of selected example ICMEs (Section 6), the primary difficulty being the availability of reliable solar data to initialise the models.
– Type II radio emissions and the interplanetary scintillation technique (Section 7) provide a means of tracking ICMEs and their associated shock waves through the region of space between the corona and 1 AU.

Despite the material presented in this chapter, there still remain many open questions on the detailed correspondence between the features and phenomena revealed in the solar and in situ observations. Some of these will be explored in the future by missions which approach closer to the Sun. These will certainly shed new light on the evolution of (I)CMEs. In the nearer future, simultaneous *in-situ* and coronagraph observations in high temporal and spatial resolution will allow detailed comparisons of the *in-situ* and remote sensing observations. The cadence of the instruments will also allow better study of the evolution of CMEs in the low corona. Observations in this region are also important for the reliable interpretation of *in-situ* characteristics subsequently measured in the interplanetary medium. Opportunities will also be available to measure the same ICME *in-situ* at different points in the inner heliosphere. Differences observed should help us to understand the evolution that takes place due the interaction of ICMEs with the structure already existing in the ambient solar wind.

Acknowledgements

N. U. Crooker acknowledges support from NASA under grant no. NNG05GD97G. J. Rodriguez-Pacheco acknowledges the support of the Spanish Ministerio de Educación y Ciencia under grant no. ESP2002-04379-C02-02.

References

Arge, C. N., Odstrcil, D., Pizzo, V. J., and Mayer, L.: 2002, in Velli, M., Bruno, R., and Malara, F. (eds.), *Solar Wind Ten*, Vol. 679 of *AIP Conference Proceedings*, Melville, NY, pp. 190–193.

Armstrong, J., and Coles, W. A.: 1972, *J. Geophys. Res.* **77**, 4602–4610.

Bale, S. D., Reiner, M. J., Bougeret, J.-L., Kaiser, M. L., Krucker, S., Larson, D. E., *et al.*: 1999, *Geophys. Res. Lett.* **26**, 1573–1576.

Balogh, A., Gosling, J. T., Jokipii, J. R., Kallenabch, R., and Kunow, H.: 1999, *Space Sciences Series of ISSI* Vol. 7, Kluwer, Dordrecht.

Behannon, K. W., Burlaga, L. F., and Hewish, A.: 1991, *J. Geophys. Res.* **96**, 21,213–21, 225.

Blanco, J. J., Cid, C., Rodriguez-Pacheco, J., Hidalgo, M., Nieves-Chinchilla, T., and Sequeriros, J.: 2003, *Geophys. Res. Abs.* **5**, 00354.

Bothmer, V.: 2003, *ESA Special Pub.* **535**, 419–428.

Bothmer, V., and Schwenn, R.: 1994, *Space Sci. Rev.* **70**, 215–220.

Bothmer, V., and Rust, D. M.: 1997, in Crooker, N. U., Joselyn, J. A., and Feynman, J. (eds.), *Coronal Mass Ejections*, Vol. 99 of *AGU Geophys. Mon.*, Washington, DC, pp. 139–146.

Bothmer, V., and Schwenn, R.: 1998, *Ann. Geophysicae* **16**, 1–24.

Breen, A. R., Riley, P., Lazarus, A. J., Canals, A., Fallows, R. A., and Linker, J., *et al.*: 2002, *Ann. Geophysicae* **20**, 1291–1309.

Burlaga, L. F.: 1975, *Space Sci. Rev.* **17**, 327–352.

Burlaga, L. F.: 1991, in Schwenn, R., and Marsch, E. (eds.), *Physics of the Inner Heliosphere 2*, Springer-Verlag, Berlin, Heidelberg, New York, pp. 1–22.

Burlaga, L. F.: 1995, *Interplanetary Magnetodynamics*, Oxford University Press, New York and Oxford.

Burlaga, L. F., Fitzenreiter, R., Lepping, R., Ogilvie, K., Szabo, A., Lazarus, A., *et al.*: 1998, *J. Geophys. Res.* **103**, 277–285.

Cane, H. V., and Richardson, I. G.: 1997, *J. Geophys. Res.* **102**, 17,445–17,449.

Cane, H. V., and Richardson, I. G.: 2003a, *J. Geophys. Res.* **108**, 1156, doi:10.1029/2002JA009817.

Cane, H. V., and Richardson, I. G.: 2003b, *Geophys. Res. Lett.* **30**, 2233, doi:10.1029/2003GL017685.

Cane, H. V., Stone, R. G., Fainberg, J., Steinberg, J. L., and Hoang, S.: 1982, *Solar Physics* **78**, 187–198.

Cane, H. V., Kahler, S. W., and Sheeley, N. R., Jr.: 1986, *J. Geophys. Res.* **91**, 13,321–13, 329.

Cane, H. V., Sheeley, N. R., Jr., and Howard, R. A.: 1987, *J. Geophys. Res.* **92**, 9869–9874.

Cane, H. V., Wibberenz, G., and Richardson, I. G.: 1997, *J. Geophys. Res.* **102**, 7075–7086.

Cane, H. V., Richardson, I. G., and von Rosenvinge, T. T.: 1998, *Geophys. Res. Lett.* **25**, 4437–4440.

Cliver, E. W.: 1995, *Eos Trans. AGU* **76(8)**, 75.

Cliver, E. W., and Ling, A. G.: 2001, *Astrophys. J. Lett.* **556**, 432–437.

Cliver, E. W., Feynman, J., and Garrett, H. B.: 1990, *J. Geophys. Res.* **95**, 17,103–17,112.

Cliver, E. W., Ling, A. G., and Richardson, I. G.: 2003, *Astrophys. J.* **592**, 574–579.

Cremades, H., and Bothmer, V.: 2004, *Astron. Astrophys.* **422**, 307–322.

Crooker, N. U.: 2000, *J. Atmos. Sol. Terr. Phys.* **62**, 1071–1085.

Crooker, N. U., and Cliver, E. W.: 1994, *J. Geophys. Res.* **99**, 23,383–23,390.

Crooker, N. U., and Horbury, T. S.: 2006, *Space Sci. Rev.* this volume, 10.1007/s11214-006-9014-0.

Crooker, N. U., Forsyth, R., Rees, A., Gosling, J. T., and Kahler, S. W.: 2004, *J. Geophys. Res.* **109**, A06110, doi:10.1029/2004JA010426.

Dalla, S., Balogh, A., Heber, B., and Lopate, C.: 2001, *J. Geophys. Res.* **106**, 5721–5730.

Dal Lago, A., Schwenn, R., and Gonzalez, W. D.: 2003, *Adv. Space Res.* **32**, 2637–2640.

Dere, K. P., Brueckner, G. E., Howard, R. A., and Michels, D. J.: 1999, *Astrophys. J.* **516**, 465–474.

Detman, T. R., Dryer, M., Yeh, T., Han, S. M., Wu, S. T., and McComas, D. J.: 1991, *J. Geophys. Res.* **96**, 9531–9540.
Eyles, C. J., Simnett, G. M., *et al.*: 2003, *Solar Phys.* **217**, 319–347.
Fenrich, F. R., and Luhmann, J. G.: 1998, *Geophys. Res. Lett.* **25**, 2999–3002.
Forbes, T. G., Linker, J. A., *et al.*: 2006, *Space Sci. Rev.*, this volume, 10.1007/s11214-006-9019-8.
Gapper, G. R., Hewish, A., Purvis, A., and Duffet-Smith, P. J.: 1982, *Nature* **296**, 633–636.
Gazis, P. R., Balogh, A., *et al.*: 2006, *Space Sci. Rev.*, this volume, 10.1007/s11214-006-9023-z.
Gibson, S., and Low, B. C.: 1998, *Astrophys. J.* **493**, 460–473.
González-Esparza, J. A., Neugebauer, M., Smith, E. J., and Phillips, J. L.: 1998, *J. Geophys. Res.* **103**, 4767–4773.
Gopalswamy, N., Lara, A., Lepping, R. P., Kaiser, M. L., Berdichevsky, D., and St. Cyr, O. C.: 2000, *Geophys. Res. Lett.* **27**, 145–148.
Gopalswamy, N., Lara, A., Yashiro, S., Kaiser, M. L., and Howard, R. A.: 2001a, *J. Geophys. Res.* **106**, 29,207–29,217.
Gopalswamy, N., Yashiro, S., Kaiser, M. L., Howard, R. A., and Bougeret, J.-L.: 2001b, *Astrophys. J.* **548**, L91–L94.
Gopalswamy, N., Yashiro, S., Michalek, G., Kaiser, M. L., Howard, R. A., Reames, D. V., *et al.*: 2002, *Astrophys. J.* **572**, L103–L107.
Gosling, J. T.: 1990, in Russell, C. T., Priest, E. R., and Lee, L. C. (eds.), *Physics of Magnetic Flux Ropes*, Vol. 58 of *AGU Geophys. Mon.*, Washington, DC, pp. 343–364.
Gosling, J. T., McComas, D. J., Phillips, J. L., and Bame, S. J.: 1991, *J. Geophys. Res.* **96**, 7831–7839.
Gosling, J. T., McComas, D. J., Phillips, J. L., and Bame, S. J.: 1992, *J. Geophys. Res.* **97**, 6531–6535.
Gosling, J. T., Riley, P., McComas, D. J., and Pizzo, V. J.: 1998, *J. Geophys. Res.* **103**, 1941–1954.
Groth, C. P. T., DeZeeuw, D. L., Gombosi, T. I., and Powell, K. G.: 2000, *J. Geophys. Res.* **105**, 25,053–25,078.
Hammond, C. M., Crawford, G. K., Gosling, J. T., Kojima, H., Phillips, J. L., Matsumoto, H., *et al.*: 1995, *Geophys. Res. Lett.* **22**, 1169–1172.
Hayashi, K., Kojima, M., Tokumaru, M., and Fujiki, K.: 2003, *J. Geophys. Res.* **108**, doi:10.1029/2002JA009567.
Hewish, A., Scott, P. F., and Willis, D.: 1964, *Nature* **203**, 1214–1217.
Hoang, S., Pantellini, F., Harvey, C. C., Lacombe, C., Mangeney, A., Meyer-Vernet, N., *et al.*: 1992, in Marsch, E., and Schwenn, R. (eds.), *Solar Wind Seven*, Pergamon Press, New York, pp. 465–468.
Hu, Y. Q.: 1998, *J. Geophys. Res.* **103**, 14,631–14,641.
Hudson, H. S., Bougeret, J.-L., and Burkepile, J.: 2006, *Space Sci. Rev.*, this volume, doi: 10.1007/s11214-006-9009-x.
Hundhausen, A. J.: 1988, in Pizzo, V. J., Holzer, T. E., and Sime, D. G. (eds.), *Proceedings of the Sixth International Solar Wind Conference, Rep. NCAR/TN-306*, Natl. Cent. for Atmos. Res., Boulder, pp. 181–214.
Huttunen, E., Schwenn, R., Bothmer, V., and Koskinen, H. E. J.: 2005, *Ann. Geophysicae* **23**, 625–641.
Jadav, R. M., Iyer, K. N., Joshi, H. P., and Vats, H. O.: 2005, *Planet. Space Sci.* **53**, 671–679.
Intriligator, D. S., Jokipii, J. R., Horbury, T., Intriligator, J. M., Forsyth, R., Kunow, H., *et al.*: 2001, *J. Geophys. Res.* **106**, 10,625–10,634.
Klein, L. W., and Burlaga, L. F.: 1982, *J. Geophys. Res.* **87**, 613–624.
Knetter, T., Neubauer, F. M., Horbury, T., and Balogh, A.: 2004, *J. Geophys. Res.* **109**, 10.1029/2003JA010099.
Knock, S. A., Cairns, I. H., Robinson, P. A., and Kuncic, Z.: 2001, *J. Geophys. Res.* **106**, 25,041–25,051.
Leamon, R. J., Smith, C. W., and Ness, N. F.: 1998, *Geophys. Res. Lett.* **25**, 2505–2508.
Lengyel-Frey, D., Stone, R. G., and Bougeret, J.-L.: 1985, *Astron. Astrophys.* **151**, 215–221.

Lengyel-Frey, D., and Stone, R. G.: 1989, *J. Geophys. Res.* **94**, 159–167.
Lindsay, G. M., Russell, C. T., Luhmann, J. G., and Gazis, P.: 1994, *J. Geophys. Res.* **99**, 11–17.
Lindsay, G. M., Luhmann, J. G., Russell, C. T., and Gosling, J. T.: 1999, *J. Geophys. Res.* **104**, 12,515–12,523.
Linker, J. A., Mikic, Z., Biesecker, D. A., Forsyth, R. J., Gibson, S. E., Lazarus, A. J., *et al.*: 1999, *J. Geophys. Res.* **104**, 9809–9830.
Liu, Y., and Hayashi, K.: 2006, *Astrophys. J.* **640**, 1135–1141.
Liu, Y., Richardson, J. D., and Belcher, J. W.: 2005, *Planet. Space Sci.* **53**, 3–17.
Malitson, H. H., Fainberg, J., and Stone, R. G.: 1973, *Astrophys. Lett.* **14**, 111–114.
Manchester IV, W. B., Gombosi, T. I., Roussev, I., DeZeeuw, D. L., Sokolov, I. V., Powell, K. G., *et al.*: 2004a, *J. Geophys. Res.* **109**, doi:10.1029/2002JA009672.
Manchester IV, W. B., Gombosi, T. I., Roussev, I., Ridley, A., DeZeeuw, D. L., Sokolov, I. V., *et al.*: 2004b, *J. Geophys. Res.* **109**, doi:10.1029/2003JA010150.
Manoharan, P. K., Tokumaru, M., Pick, M., Subramanian, P., Ipavich, F. M., Schenk, K., *et al.*: 2001, *Astrophys. J.* **559**, 1180–1189.
Marsch, E.: 1991, in Schwenn, R., and Marsch, E. (eds.), *Physics of the Inner Heliosphere 1*, Springer-Verlag, Berlin, Heidelberg, New York, pp. 159–241.
McComas, D. J., Gosling, J. T., Hammond, C. M., Moldwin, M. B., Philips, J. L., and Forsyth, R. J.: 1994, *Geophys. Res. Lett.* **21**, 1751–1754.
Mikic, Z., and Lee, M. A.: 2006, *Space Sci. Rev.*, this volume, doi: 10.1007/s11214-006-9012-2.
Moldwin, M. B., Phillips, J. L., Gosling, J. T., Scime, E. E., McComas, D. J., Balogh, A., *et al.*: 1995, *J. Geophys. Res.* **100**, 19,903–19,910.
Mulligan, T., Russell, C. T., and Luhmann, J. G.: 1998, *Geophys. Res. Lett.* **25**, 2959–2962.
Odstrcil, D., Dryer, M., and Smith, Z.: 1996, *J. Geophys. Res.* **101**, 19,973–19,986.
Odstrcil, D., and Pizzo, V. J.: 1999a, *J. Geophys. Res.* **104**, 483–492.
Odstrcil, D., and Pizzo, V. J.: 1999b, *J. Geophys. Res.* **104**, 493–503.
Odstrcil, D., Riley, P., and Zhao, X. P.: 2004, *J. Geophys. Res.* **109**, A02116, doi:10.1029/2003JA010135.
Odstrcil, D., Pizzo, V. J., and Arge, C. N.: 2005, *J. Geophys. Res.*, **110**, A02106, doi:10.1029/2004JA010745.
Pick, M., Forbes, T. G., *et al.*: 2006, *Space Sci. Rev.*, this volume, doi: 10.1007/s11214-006-9021-1.
Reiner, M. J., Kaiser, M. L., Fainberg, J., Bougeret, J.-L., and Stone, R. G.: 1997, *Proceedings of the 31st ESLAB Symposium, ESA SP-415*, 183–188.
Reiner, M. J., Kaiser, M.L., Fainberg, J., and Stone, R. G.: 1998, *J. Geophys. Res.* **103**, 29,651–29,664.
Reiner, M. J., Kaiser, M. L., Fainberg, J., and Stone, R. G.: 1999, in Habbal, S. R., Esser, R., Hollweg, J. V., and Isenberg, P. A. (eds.) *Solar Wind Nine*, Vol. 471 of *AIP Conference Proceedings* Woodbury, NY, pp. 653–656.
Reiner, M. J., Kaiser, M. L., Karlický, M., Jiřička, K., and Bougeret, J.-L.: 2001, *Solar Phys.* **204**, 123–139.
Reiner, M. J., Kaiser, M. L., and Bougeret, J.-L.: 2003, in Velli, M., Bruno, R., and Malara, F. (eds.), *Solar Wind Ten*, Vol. 679 of *AIP Conference Proceedings*, Melville, NY, pp. 152–155.
Reiner, M. J., Jackson, B. V., Webb, D. F., Mizuno, D. R., Kaiser, M. L., and Bougeret, J.-L.: 2005, *J. Geophys. Res.* **110**, doi:10.1029/ 2004JA010943.
Richardson, I. G., and Cane, H. V.: 2005, *Geophys. Res. Lett.* **32**, L02104, doi:10.1029/2004GL021691.
Richardson, I. G., Cliver, E. W., and Cane, H. V.: 2001, *Geophys. Res. Lett.* **28**, 2569–2572.
Richardson, I. G., Cane, H. V., and Cliver, E. W.: 2002, *J. Geophys. Res.* **107**, 10.1029/2001JA000504.
Richardson, I., Lawrence, G. R., Haggerty, D. K., Kucera, T. A., and Szabo, A.: 2003, *Geophys. Res. Lett.*, **30**, 8014, doi:10.1029/2002GL016424.

Riley, P., Gosling, J. T., and Pizzo, V. J.: 1997, *J. Geophys. Res.* **102**, 14,677–14,686.
Riley, P., Linker, J. A., and Mikic, Z.: 2001, *J. Geophys. Res.* **106**, 15,889–15,901.
Rodriguez-Pacheco, J., Blanco, J. J., and Crooker, N. U.: 2005, unpublished manuscript.
Rogers, B. N., Drake, J. F., and Shay, M. A.: 2000, *Geophys. Res. Lett.* **27**, 3157–3160.
Roussev, I. I., Gombosi, T. I., Sokolov, I. V., Velli, M., Manchester IV, W., DeZeeuw, D. L., *et al.*: 2003, *Astrophys. J.* **595**, L57–L61.
Roussev, I. I., Sokolov, I. V., Forbes, T. G., Gombosi, T. I., Lee, M. A., and Sakai, J. I.: 2004, *Astrophys. J.* **605**, L73–L76.
Russell, C. T., Mulligan, T., and Anderson, B. J.: 2003, in Velli, M., Bruno, R., and Malara, F. (eds.), *Solar Wind Ten*, Vol. 679 of *AIP Conference Proceedings*, Melville, NY, pp. 121–124.
Ruzmaikin, A., Feynman, J., and Smith, E. J.: 1997, *J. Geophys. Res.* **102**, 19,653–19,759.
Schmidt, J. M.: 2000, *Sol. Phys.* **197**, 135–184.
Schmidt, J. M., and Cargill, P. J.: 2001, *J. Geophys. Res.* **106**, 8283–8289.
Schmidt, J. M., and Cargill, P. J.: 2003, *J. Geophys. Res.* **108**, 1023, doi:10.1029/2002JA009325.
Schmidt, J. M., and Cargill, P. J.: 2004, *Annales Geophys.* **22**, 2245–2254.
Schwenn R.: 1986, *Space Sci. Rev.* **44**, 139–168.
Schwenn, R.: 1990, in Schwenn, R., and Marsch, E. (eds.), *Physics of the Inner Heliosphere 1*, Springer-Verlag, Berlin, Heidelberg, New York, pp. 99–181.
Schwenn, R., Dal Lago, A., Huttunen, E., and Gonzales, W. D.: 2005, *Ann. Geophysicae* **23**, 1033–1059.
Schwenn, R., Raymond, J. C., *et al.*: 2006, *Space Sci. Rev.*, this volume, doi: 10.1007/s11214-006-9016-y.
Sheeley, N. R., Jr., Howard, R. A., Koomen, M. J., Michels, D. J., Schwenn, R., Mühlhäser, K. H., *et al.*: *J. Geophys. Res.* **90**, 163–175.
Smith, C. W., and Phillips, J. L.: 1997, *J. Geophys. Res.* **102**, 249–261.
Tokumaru, M., Kojima, M., Fujiki, K., Yamashita, M., and Yokobe, A.: 2003, *J. Geophys. Res.* **108**, 1220, doi:10.1029/2002JA009574.
Tokumaru, M., Kojima, M., Fujiki, K., Yamashita, M., and Baba, D.: 2005, *J. Geophys. Res.* **110**, A01109, doi:10.1029/2004JA010656.
Totten, T. L., Freeman, J. W., and Arya, S.: 1995, *J. Geophys. Res.* **100**, 13–17.
Usmanov, A. V., Goldstein, M. L., Besser, B. P., and Fritzer, J. M.: 2000, *J. Geophys. Res.* **105**, 12,675–12,696.
Vandas, M., Odstrcil, D., and Watari, S.: 2002, *J. Geophys. Res.* **107**, doi:10,1029/2001JA005068.
Vasquez, B. J., Farrugia, C. J., Markovskii, S. A., Hollweg, J. V., Richardson, I. G., Ogilvie, K. W., *et al.*: 2001, *J. Geophys. Res.* **106**, 29,283–29,298.
Wang, C., Du, D., and Richardson, J. D.: 2005, *J. Geophys. Res.* **110**, doi:10.1029/2005JA011198.
Webb, D. F., and Howard, R. A.: 1994, *J. Geophys. Res.* **99**, 4201–4220.
Webb, D. F., Cliver, E. W., Gopalswamy, N., Hudson, H. S., and St. Cyr, O. C.: 1998, *Geophys. Res. Lett.* **25**, 2469–2472.
Webb, D. F., Lepping, R. P., Burlaga, L. F., DeForest, C. E., Larson, D. E., Martin, S. F., *et al.*: 2000, *J. Geophys. Res.* **105**, 27,251–27,259.
Wibberenz, G., Richardson, I. G., and Cane, H. V.: 2002, *J. Geophys. Res.* **107**, doi: 10.1029/2002JA009461.
Wimmer-Schweingruber, R. F., Crooker, N. U., *et al.*: 2006, *Space Sci. Rev.*, this volume, doi:10.1007/s11214-006-9017-x.
Woo, R.: 1988, *J. Geophys. Res.* **93**, 3919–3926.
Woo, R., and Schwenn, R.: 1991, *J. Geophys. Res.* **96**, 21,227–21,244.
Zhao, X. P.: 1992, *J. Geophys. Res.* **97**, 15,051–15,055.

Zhao, X. P., and Hoeksema, J. T.: 1996, *J. Geophys. Res.* **101**, 4825–4834.
Zhao, X. P., and Hoeksema, J. T.: 1997, *Geophys. Res. Lett.* **24**, 2965–2968.
Zhao, X. P., and Webb, D. F.: 2003, *J. Geophys. Res.* **108**, 1234, doi:10.1029/2002JA009606.
Zhao, X. P., Plunkett, S. P., and Liu, W.: 2002, *J. Geophys. Res.* **107**, doi:10,1029/2001JA009143.
Zhang, J., Dere, K. P., Howard, R. A., and Bothmer, V.: 2003, *Astrophys. J.* **582**, 520–533.
Zurbuchen, T. H., and Richardson, I. G.: 2006, *Space Sci. Rev.*, this volume, doi: 10.1007/s11214-006-9010-4.